



Deposited via The University of Sheffield.

White Rose Research Online URL for this paper:

<https://eprints.whiterose.ac.uk/id/eprint/127832/>

Version: Accepted Version

Article:

Kirby, M.E., Heusser, L., Scholz, C. et al. (2018) A late Wisconsin (32–10k cal a BP) history of pluvials, droughts and vegetation in the Pacific south-west United States (Lake Elsinore, CA). *Journal of Quaternary Science*, 33 (2). pp. 238-254. ISSN: 0267-8179

<https://doi.org/10.1002/jqs.3018>

Reuse

Items deposited in White Rose Research Online are protected by copyright, with all rights reserved unless indicated otherwise. They may be downloaded and/or printed for private study, or other acts as permitted by national copyright laws. The publisher or other rights holders may allow further reproduction and re-use of the full text version. This is indicated by the licence information on the White Rose Research Online record for the item.

Takedown

If you consider content in White Rose Research Online to be in breach of UK law, please notify us by emailing eprints@whiterose.ac.uk including the URL of the record and the reason for the withdrawal request.

1 **A late Wisconsin (32-10k cal a BP) history of pluvials, droughts, and vegetation in the**
2 **Pacific southwest United States (Lake Elsinore, CA).**

3
4
5
6

*Kirby, M.E.^a, Heusser, L.^b, Scholz, C.^c, Ramezan, R.^d, Anderson, M.A.^e, Markle B.^f, Rhodes,
E.^g, Glover, K.A.^h, Fantozzi, J.^a, Hiner, C.^a, Price, B.^a, Rangel, H.^a

7 ^a *Department of Geological Sciences, California State University, Fullerton, Fullerton, CA*
8 *92834 USA (mkirby@fullerton.edu);* ^b *Lamont-Doherty Earth Observatory of Columbia*
9 *University, Palisades, NY 10601 (heusser@ldeo.columbia.edu), USA;* ^c *Department of Earth*
10 *Sciences, Syracuse University, Syracuse, NY USA 13244 (cascholz@syr.edu);* ^d *Department of*
11 *Mathematics, California State University, Fullerton, Fullerton, CA 92834,* ^e *University of*
12 *California Riverside, Department of Environmental Sciences, Riverside, CA 92521;* ^f
13 *Quaternary Research Center and Department of Earth and Space Sciences, University of*
14 *Washington, Seattle, Washington 98195, USA (bradley.markle@gmail.com);* ^g *Geography,*
15 *University of Sheffield, Sheffield, United Kingdom (ed.rhodes@sheffield.ac.uk);* ^h *Climate*
16 *Change Institute, University of Maine, Orono, ME 04469 (katherine.glover@maine.edu).*

17
18
19

*corresponding author

20 **Running Head:** California's glacial history of pluvials, droughts, and vegetation

21

22 **Keywords:** Lakes, sediment, Glacial, California, drought, insolation

23

24 **ABSTRACT:** Continuous, sub-centennially resolved, paleo terrestrial records are rare from arid
25 environments such as the Pacific southwest United States. Here, we present a multi-decadal-to-
26 centennial resolution sediment core (Lake Elsinore, CA) to reconstruct late Wisconsin pluvials,
27 droughts, and vegetation. In general, the late Wisconsin is characterized by a wetter and colder
28 climate than during the Holocene. Specifically, conditions between 32.3-24.9k cal a BP are
29 characterized by large amplitude hydrologic and ecologic variability. Highlighting this period is
30 ~2000-year glacial mega-drought (27.6-25.7k cal a BP) during which the lake shallowed (3.2-4.5
31 m depth). This period is approximately coeval to a Lake Manix regression and an increase in

32 xeric vegetation in the San Bernardino Mountains (Baldwin Lake). The Local Last Glacial
33 Maximum (LLGM) is bracketed between 23.3-19.7k ca a BP – a ~3000-year interval
34 characterized by reduced run-off (relative to the glacial), colder conditions, and vegetative
35 stability. Maximum sustained wetness follows the LLGM, beginning at 19.7 and peaking by
36 14.4k cal a BP. A two-step decrease in runoff characterizes the late glacial to Holocene
37 transition; however, the vegetation change is more complex, particularly at the beginning of the
38 Younger Dryas chronozone. By 12.6-12.4k cal a BP, the climate achieved near Holocene
39 conditions.

40

41

42 **Introduction and Background**

43

44 The Pacific southwest United States (pswUS) is a perennially water-stressed and over-populated
45 region. This stress is unlikely to diminish in the future as droughts become more frequent and
46 severe (Neelin et al., 2013; Seager et al., 2013; Kam and Sheffield, 2016). At the same time, the
47 intensity of precipitation could increase as well, exacerbating risk associated with floods and
48 their related hazards (Berg and Hall, 2015; Yoon et al., 2015; Shields and Kiehl, 2016).

49 Preparing for these scenarios and mitigating their impact is key to maintaining the region's
50 population and its socioeconomic vitality. Key to preparation and mitigation is a paleo
51 perspective. Paleo perspectives inform on the range of climatic possibilities such as drought and
52 floods. Included in this paleo perspective is the role that changes in climate play on vegetative
53 structure. In the pswUS, native vegetation is highly stressed resulting in its inclusion as one of
54 the world's 25 biodiversity hotspots (Myers et al., 2000). Known as the California Floristic
55 Biodiversity Hot Spot, this region is experiencing, and will continue to experience, threats
56 associated with climate change. In this paper, we use sediments from Lake Elsinore, California
57 to gain paleo perspectives on hydroclimates and their relationship to vegetation between 32 and
58 10k cal a BP. Specifically, we build on, and add to, existing vegetative (32.6-9k cal a BP,
59 Heusser et al., 2015) and the deglacial (19-9k cal a BP, Kirby et al., 2013) reconstructions by
60 updating the age model, adding indicators of runoff from 32-17k cal a BP, and examining the
61 relationship between the runoff and vegetation between 32-10k cal a BP. We focus specifically
62 on a prolonged dry interval between 27.6-25.7k cal a BP, with consideration for regional

63 comparisons. We begin this paper with a brief review of Kirby et al. (2013) and Heusser et al.
64 (2015).
65
66 Kirby et al. (2013) document the late glacial to Holocene transition (19-9k cal a BP) using a
67 combination of sediment grain size to infer runoff and C₂₈ *n*-alkanoic acids from plant leaf waxes
68 (δD_{wax}) to infer moisture source. In general, runoff decreases from 19-9k cal a BP with notable
69 shifts to less runoff at the start of the Bolling-Allerod (B-A) (14.7k cal a BP) and then again at
70 the start of the Younger Dryas (YD) (12.9k cal a BP). A comparison to known forcings such as
71 the Atlantic Meridional Overturning Circulation (AMOC), ice sheet area, and CO₂ radiative
72 forcing reveal potential causative relationships. Notably, the long term decrease in wetness from
73 19-9k cal a BP mirror both loss of ice sheet volume and an increase in CO₂ radiative forcing.
74 Together, these changes may have gradually shifted the mean winter storm track north from 19-
75 9k cal a BP. Alternatively, the storm track may have experienced very little latitudinal changes,
76 instead reflecting a change in the frequency and/or intensity of southward tracking storms as
77 climate transitioned from a glacial state to a Holocene state (Antevs, 1948; Wells et al., 2003;
78 Kirby et al., 2013; Ibarra et al., 2014; Löfverström et al., 2014; Oster et al., 2015; Wong et al.,
79 2016; Lora et al., 2016). The δD_{wax} mirror this gradual decrease in wetness suggesting a change
80 in dominant moisture sources from higher latitude sourced (or colder storms) to lower latitude
81 sourced (or warmer storms) winter storms between 19-9k cal a BP. The δD_{wax} do not indicate a
82 tropical or subtropical moisture source during the late glacial as proposed by Lyle et al. (2012).
83 Superimposed on this gradual drying trend are shifts in wetness at 14.7 and 12.9k cal a BP.
84 These shifts are proposed to be coeval to shifts in AMOC strength. Consequently, the pswUS
85 late glacial to Holocene transition is likely forced by a combination of external drivers associated
86 with ice sheet dynamics and radiative forcing as well as oceanic forcing associated with
87 conditions in the North Atlantic.
88
89 Heusser et al. (2015) examine the pollen data between 32.6-9k cal a BP. Results show a
90 generally more mesic vegetation than today during the last glacial. Evidence for shifts in
91 vegetation, particularly between 27.5-25.5k cal a BP (27.6-25.7k cal a BP as per updated age
92 model – this paper), suggest a significant vegetative response. The latter 2000-year interval is
93 interpreted as a return to more xeric vegetation reflecting a more arid climate. A comparison to

94 pollen from Santa Barbara Basin show generally similar millennial scale features as Lake
95 Elsinore (Heusser, 1995; Heusser and Sirocko, 1997). However, as Heusser et al. (2015) notes,
96 the 2000-yr glacial mega-drought is missing from the Santa Barbara Basin pollen record,
97 suggesting that the terrestrial Lake Elsinore pollen site may capture changes absent in its marine
98 counterpart (Heusser, 1995; Heusser and Sirocko, 1997).

99

100

101 **Study Site**

102

103 *Modern climate setting*

104

105 The climate of the pswUS is Mediterranean, characterized by wet, cool winters and hot, dry
106 summers. In general, the coastal plain and low-lying inland regions receive less precipitation
107 than the adjacent mountain ranges (Masi, 2005). In particular, tropical (El Niño Southern
108 Oscillation (ENSO)) and extratropical (Pacific Decadal Oscillation (PDO)) Pacific Ocean-
109 atmosphere conditions influence the climate of the pswUS (Cayan and Peterson, 1989; Cayan et
110 al., 1999; Brito-Castillo et al., 2003; Hanson et al., 2006). Pacific Ocean-atmosphere conditions
111 modulate the mean winter position of the eastern Pacific subtropical high (Cayan and Peterson,
112 1989; Hanson et al., 2006). When the jet stream is south it results in higher than average
113 precipitation and associated river discharge, while a more northerly position of the jet stream
114 results in lower than average precipitation and less river discharge (Cayan et al., 1999; Hanson et
115 al., 2006). Most importantly for our paleo studies is that the pswUS is a relatively simple,
116 unimodal precipitation regime as compared to its interior southwest US counterparts (Kirby et
117 al., 2013). Consequently, the hydroclimatic paleo interpretation is straightforward – indicators of
118 wet climates are caused by wetter winters and vice versa for dry climate indicators. Finally, it is
119 well documented that changes in precipitation in the pswUS are positively correlated to both
120 changes in regional lake level and changes in the flux, and size, of sediment in regional rivers,
121 illustrating the modern link between climate and sedimentation in the study region (Inman and
122 Jenkins, 1999; Warrick et al., 2004, 2007, 2015; Romans et al., 2009; Covault et al., 2010; Xu et
123 al., 2010; Kirby et al., 2010, 2013, 2014; Gray et al., 2014, 2015; Hiner et al., 2016).

124

125 *Tectonic setting*

126

127 Lake Elsinore is a pull-apart basin along the Elsinore Fault zone formed by fault step-over
128 movement along the strike-slip Wildomar Fault to the Glen Ivy North Fault (Mann, 1956; Hull,
129 1990) (Figure 1). Gravimetric studies reveal an approximately 1000 m thick sediment package
130 within the basin (Hull, 1990). The basement rocks are granitic and date to the late Cretaceous
131 (Krummenacher et al., 1975; Silver et al., 1979).

132

133 At Lake Elsinore fault dip is near vertical and seismic activity is low (Krummenacher et al.,
134 1975). Only two moderate earthquakes have been recorded in the northern Elsinore fault zone
135 over the past 200 years ($M \leq 6$, Topozada et al., 1978). Along the southern section of the
136 Elsinore fault zone, approximately 40 km to the SE of Lake Elsinore, a minimum of four
137 earthquakes ($M \leq 4.5$) have generated surface rupture over the last 4,500 years (Vaughan et al.,
138 1999). Available data on fault slip rates suggest that the horizontal to vertical slip ratio is in
139 excess of 10:1 (Hull and Nicholson, 1992). Horizontal separation is estimated at 10 to 15 km
140 over the past ~ 2.5 Ma based on offset features observed in bedrock, most notably changes in
141 foliation dip; only minimal vertical offset has been identified (Weber, 1977; Morton and Miller,
142 1987).

143

144 From this tectonic interpretation, it is concluded that hydrologically-produced, vertical changes
145 in the lake's base level greatly exceed earthquake-generated vertical changes. Under modern
146 conditions, these hydrologically-produced changes can exceed 13 m (Kirby et al., 2004). In other
147 words, complete desiccation of modern Lake Elsinore results from a 13 m drop in base-level
148 (Kirby et al., 2004). Vertical changes due to fault rupture are small ($< 1-2$ m) based on paleo
149 seismic data (Vaughan et al., 1999). This extreme disparity between hydrologic and tectonic
150 forced base level change suggests that vertical motion related to tectonics is not the primary
151 determiner of the lake's changing sedimentation and stratal geometries, especially over the
152 geologically short periods of time analyzed in this paper. Of course, on longer timescales, the
153 basin's rate of fault-related vertical subsidence must exceed average sedimentation rates in order
154 for the basin to exist as depositional feature. As a test of this statement, we collected seismic

155 reflection data to examine the basin's long-term sedimentation and stratal geometries, with the
156 purpose to identify potential basin faulting and its influence on sedimentation (see Discussion).

157

158 *Limnology*

159

160 Lake Elsinore is a shallow, polymictic lake (Anderson, 2001). The hypolimnion experiences
161 short periods of anoxia, but wind mixing of epilimnic oxygen rich waters into the hypolimnion
162 inhibits prolonged anoxia, under modern conditions (Anderson, 2001). The occurrence of
163 laminae during parts of the glacial suggest a deeper lake (perhaps anoxic) at times (Kirby et al.,
164 2013). The lake's water budget is controlled by a combination of outputs such as evaporation,
165 ($>1.4 \text{ m yr}^{-1}$, Anderson, 2001) and occasional overflow. Inputs include direct runoff from its
166 main influent, the San Jacinto River, as well as runoff from the adjacent Elsinore Mountains. The
167 role ground water plays in the lake's hydrologic budget is less well known (Damiata and Lee,
168 1986; Thiros, 2010). The main outlet is located along the north side of the lake. Twenty brief
169 overflow events into northwest flowing Walker Canyon have occurred since 1769 AD, including
170 three times in the 20th century (Lynch, 1931). Consequently, the lake is sometimes a terminal
171 basin (closed) and at other times a through-flow basin (open). Modern maximum lake level depth
172 is $\sim 13 \text{ m}$ before overflow occurs, based on the modern sill elevation (Anderson, 2001). It is
173 unknown how the spill elevation has changed through geologic time. Historically the lake has
174 desiccated on several occasions since 1769 AD, most recently in the 1950's (Lynch, 1931).
175 During the 1950's drying episode, the lake's central basin remained a wet, muddy environment
176 (Hudson, 1978). The 1950's drying event is recognized in sediment cores as a low water content,
177 stiff crumbly clayey-silt unit with low sand content (Kirby et al., 2004, 2010).

178

179

180 **Methods**

181

182 *Age control*

183

184 Twenty-eight AMS radiocarbon ages on discrete organics (e.g., wood, charcoal), bulk $C_{org.}$,
185 gastropod shells, or paired discrete-bulk $C_{org.}$ materials were measured at the University of

186 California, Irvine W. M. Keck Carbon Cycle Accelerator Mass Spectrometry Laboratory or the
187 Lawrence Livermore National Laboratory (Table 1). Discrete and bulk C_{org} samples were
188 prepped using a standard acid-base-acid pretreatment. The gastropod shells were leached of 50%
189 of their mass using HCl to remove secondary carbonate. Two Infra-Red Stimulated
190 Luminescence (IRSL) dates from single grains (175–200 µm) of K-feldspar were obtained from
191 two silty-sand units (2438 – 2452 cm and 2500 – 2517 cm) at the University of California, Los
192 Angeles following standard lab protocol (Rhodes, 2015). An age model was created using 28
193 radiocarbon ages entered into the Bacon (v.2.2, IntCal13) age-modelling software (Blaauw and
194 Christen 2011) (Table 1). The IRSL ages are not included in the age model calculation.

195

196 *Sediment and pollen analyses*

197

198 Core LEDC10-1 was extracted from 7 m water depth over three days in June 2010 using a
199 hollow stemmed auger push core system with a lined hole aboard a stabilized coring barge
200 (Figure 1). Each drive was 0.61 m and recovery was better than 90% for the total core length.
201 Core acquisition started at 9 m below the sediment-water interface and ended at 30 m. The cores
202 were capped, labeled and transported back to the Cal State Fullerton Lab where they were opened,
203 described, and digitally photographed. 4-5 grams of wet sediment was extracted at 1 cm
204 contiguous intervals for magnetic susceptibility measurements, percent total organic matter (LOI
205 550 °C), and percent total carbonate (LOI 950 °C). Samples for grain size analysis were
206 extracted every other cm for determination using a Malvern laser diffraction grain size analyzer.
207 Each grain size sample was pretreated using 30 mL 30% H₂O₂ to remove organic matter, 10 mL
208 1N HCl for carbonate removal, and 10 mL 1N NaOH for biogenic silica removal. Complete
209 measurement details for all sediment analyses are provided in Kirby et al. (2013). The same set
210 of grain size methods were determined for the surface sediment samples collected by Anderson
211 (2001). Pollen methods, results, and statistical analyses are described in Heusser et al. (2015).

212

213 To determine statistically significant break-points in the percent total sand data, we use a
214 sequential regime shift detection program (SRSD v.6.2
215 <https://sites.google.com/site/climatologic/>) by Rodionov (2004, 2015) – the same as that used by
216 Kirby et al. (2014) for Zaca Lake. The data were separately analyzed pre- and post- 27.6-25.7k

217 cal a BP to avoid the exceptionally high sand content unit. Targeted significance level was $p <$
218 0.05 with a cut-off data point length of 20 and a Huber's tuning constant of 2. Red noise
219 estimation was not included (Rodionov, 2004, 2015). The purpose of this analysis is to provide a
220 statistical (non-subjective) basis for subdividing the sand data into statistically significant
221 intervals. This method removes the subjectivity often associated with visually assigned break
222 points in otherwise complex, variable time series data. Because the grain size data were sampled
223 at a higher resolution than the pollen data, we use the SRSD intervals (rather than the pollen
224 zones from Heusser et al., 2015) as the focus of our discussion section.

225
226 Modern lake bottom surface sand values were plotted versus modern water depth (ca. 2001 AD)
227 and analyzed using nonlinear regression with bootstrap confidence intervals. Following least
228 squares approach, the parametric curve $Depth = b_0 + b_1(\text{percent total sand})^{b_2}$ was fitted to
229 the data. The quantiles of 1,000 bootstrap samples were used to estimate the uncertainty around
230 the fitted model. Grain size distributions were also plotted for a modern Lake Elsinore beach
231 sample and for all modern lake bottom sediment samples between 6.01 and 7.32 m water depth.
232 The same plots were made for SRSD intervals 1-7 and 9-14 as well as SRSD 8 – the glacial sand
233 unit.

234 235 *Seismic reflection data*

236
237 Twenty high-resolution single-channel seismic reflection profiles, totaling ~ 75 km in length,
238 were used to investigate Lake Elsinore's sub bottom (Figure 1). Seismic reflection profiles were
239 collected using both a shallow, high-resolution system (4-24 kHz CHIRP) and a deeper-
240 penetrating, lower-frequency source system (1 kHz Boomer), with position information provided
241 by a differential GPS navigation system. The 1kHz seismic data were recorded digitally at a
242 sampling interval of 0.125 ms. A velocity of 1500 m/sec was used for data processing (Scholz,
243 2001). Raw seismic data files were transferred into ProMax seismic processing software. Raw
244 data were processed using four separate filters (Yilmaz, 2001). A spiking/ predictive
245 deconvolution and a bandpass filter were used to attenuate ringing of the shallow water data sets
246 and eliminate extraneous coherent noise. A trace-mixing filter was applied to the seismic data to
247 further diminish random noise and enhance signals from the sedimentary record. In addition, an

248 automatic gain control function, which counteract the natural attenuation of the seismic signal
249 with depth, was used to enhance the later (deeper) seismic arrivals. Processed lines were
250 transferred to Seisworks-2D for final seismic reflection analysis and interpretation.

251

252

253 **Results**

254

255 *Age control*

256

257 The twenty-eight, radiocarbon based age model is updated from Kirby et al. (2013) and Heusser
258 et al. (2015) (Figure 2, Table 1). Figure 2b and 2c show the differences between the former age
259 model used by Kirby et al. (2013) and Heusser et al. (2015) and that determined for this paper.
260 Importantly, this updated age model does not invalidate interpretations in Kirby et al. (2013) or
261 Heusser et al. (2015). For example, the absolute ages of the pollens zones determined in the
262 Heusser et al. (2015) paper move up-time or down-time respectively; however, the statistical
263 basis for these pollen zones is time independent. Three bulk organic carbon dates used in Kirby
264 et al. (2013) and Heusser et al. (2015) are not used in this paper's age model (1747-1748 cm,
265 1823-1824 cm, and 2019-2020 cm). Eight new age control points are added to this paper
266 including: 1723-1725 cm, 2280-2282 cm, 2292-2293 cm, 2384-2386 cm, 2425-2427 cm, 2830-
267 2832 cm, and 2 x 2860-2861 cm (Table 1). Overall, the age model indicates relatively linear
268 sedimentation between 32-10k cal a BP ($0.08 \text{ cm}^{-1} \text{ year}$ or $13.1 \text{ years cm}^{-1}$).

269

270 *Sedimentology*

271

272 Core LEDC10-1 consists predominantly of clayey silts with minor sand contributions (< 20 %)
273 (Figure 3 and S1). The average time step between individual grain size analyses is 30 years
274 (Figure S2). Organic matter and carbonate make up less than < 20 % of the total sediment
275 material, in general. The sediment is variably laminated in places and occasionally massive
276 (Figure 3). A notable increase in organic matter occurs between ~25-23k cal a BP and to a lesser
277 extent between 31-30k cal a BP. Carbonate is virtually absent between 32-14k cal a BP;
278 however, it increases dramatically at ~14k cal a BP and into the Holocene (Kirby et al., 2007,

279 2013). A distinct sand-dominated unit occurs between 27.6-25.7k cal a BP (Figure 3 and S1).
280 SRSD analysis defines thirteen statistically significant ($p < 0.05$) break points in the sand data.
281 We assign the glacial sand layer its own interval, thus bringing the total defined sand intervals to
282 fourteen (Figure 4). All of SRSD sand intervals, except the youngest (1) and the oldest (14),
283 average percent total sand values higher than the Holocene average (Figure 4). Modern lake
284 bottom sediment samples reveal a decrease in total sand with increasing water depth (Figure 5).
285 Grain size plot distributions show that silty clay dominates the modern lake bottom samples
286 between 6.01 and 7.32 m water depth as well as the SRSD intervals 1-7 and 9-14 (Figure 6).
287 Conversely, the modern beach sample and glacial sand unit (SRSD 8) are coarser, characterized
288 by sand and sandy silt, respectively. Pollen results are discussed in detail by Heusser et al.
289 (2015). The average time step between individual pollen analyses is 92 years with intervals of
290 higher resolution data across zones of interest (Figure S2).

291

292 *Seismic reflection data*

293

294 Two representative seismic reflection lines acquired using the 1 kHz Boomer system are shown
295 on Figure 7. LE line 10 was collected along the lake's long axis while LE line 33 was collected
296 along the short axis. The two lines intersect very near the core location used for this study
297 (Figure 1, LEDC10-1). Image quality diminishes with depth, likely the result of gas-produced
298 signal attenuation. Nonetheless, faint sub-parallel reflectors are observed to about 60-70 m below
299 the lake bottom. In general, the two lines show moderate divergent basin fill stratal geometries
300 with parallel to sub-parallel reflectors (Figure 7).

301

302

303 **Discussion**

304

305 *Basin analysis*

306

307 The seismic reflection data reveal a basin fill geometry typically associated with pull-apart
308 basins such as moderate divergent fill geometries characteristic of sediment focusing (Figure 7)
309 (Blais and Kalff, 1995; Csato et al., 1997; Enzel et al., 2006). Reflectors are strongest in the

310 upper 10 m of the sediment package, corresponding to the Holocene. Within the upper 10 m,
311 there is some evidence for laterally discontinuous reflectors, possibly truncation and offlapping,
312 suggesting periods of lake surface area contraction (i.e., low lake level) (Kirby et al., 2004; Pyke,
313 2013). Reflectors deeper than 10 m (glacial-age), are less prominent, exhibit less divergence, and
314 are more laterally continuous in terms of stratal thickness. This change from the Holocene to the
315 glacial likely reflects the generally wetter glacial climate and the subsequently larger lake surface
316 area associated with greater runoff (see discussion below). As a result, the area of sedimentation
317 expanded within the glacial basin creating a more uniformly thick sediment package with little
318 expression of tapering shoreward. At the time of data acquisition, the lake's surface elevation
319 was unusually low; consequently, we were unable to collect data at the far edges of the basin
320 where lateral displacement associated with the Wildomar or Glen Ivy faults is anticipated (Figure
321 1). Importantly, there is no evidence of central-basin faulting, large-scale erosional truncation, or
322 prograding clinoforms (deltaic migration). The absence of these features suggests that the
323 sediment core contains a relatively continuous sediment history.

324

325 *A late Wisconsin (32-10k cal a BP) history of pluvials, droughts, and vegetation,*
326 *with some thoughts on forcings*

327

328 *Proxy Interpretations*

329

330 *Sand as a hydrologic indicator*

331

332 In Mediterranean climates such as pswUS, the mobilization and transport of sediment,
333 particularly coarse sediment (i.e., sand size), is strongly linked to precipitation-related run-off
334 (Inman and Jenkins, 1999; Farnsworth and Milliman, 2003; Warrick and Mertes, 2009; Covault
335 et al., 2010; Xu et al., 2010; Warrick and Barnard, 2012; Gray et al., 2014; Warrick et al., 2015).
336 Research on the rivers of the pswUS confirms this strong connection to climate at both
337 interannual and multi-decadal timescales. Scaling up, it is reasonable to conclude that
338 hydroclimatic processes control the sediment mobilization signal at centennial to millennial
339 timescales for the study region as well (Romans et al., 2009; Covault et al., 2010). This
340 sediment-climate connection is manifest through increases in river discharge and enhanced

341 coarse sediment mobilization and transport during individual wetter-than-average winters or
342 intervals of wetter-than-average winters associated with changes in the mean climate state
343 (Inman and Jenkins, 1999; Farnsworth and Milliman, 2003; Romans et al., 2009; Covault et al.,
344 2010). Considering these modern studies, Kirby et al. (2010) compared percent sand, Lake
345 Elsinore lake level, San Jacinto River discharge, and the PDO index over the 20th century. Their
346 analysis revealed that small changes in sand content (generally < 15-20 %) shows a positive
347 correlation with the San Jacinto River discharge, Lake Elsinore lake level, and the PDO index. In
348 other words, greater river discharge (and higher lake levels) are associated with higher sand
349 content and vice versa. A similar 20th century comparison between percent sand and river
350 discharge was observed for Zaca Lake, also in the pswUS (Kirby et al., 2014).

351
352 From these modern and 20th century studies, we contend that the predominant driver of changes
353 in coarse sediment in pswUS lakes is hydroclimate, particularly winter season precipitation
354 variability linked to overall winter wetness. Therefore, we interpret higher percent total sand as
355 reflecting greater precipitation-related runoff (i.e., intensity and/or storm duration) and vice
356 versa. Of course, we cannot assign a specific wetness value to percent sand; however, we can use
357 changes in percent sand as a scaling tool for relative changes in wetness. In other words, higher
358 percent sand content is interpreted to reflect relatively wetter conditions and vice versa for lower
359 percent sand.

360
361 Therefore, throughout the discussion below, we use low percent sand values to infer intervals of
362 diminished runoff and thus drier climates and vice versa for high percent sand (Figure 4) (Kirby
363 et al., 2010, 2013, 2014). Our interpretation, however, of the sand data is based on small changes
364 in ambient, or background level, sand – values that range between 0 and 20 percent total sand,
365 generally (Figure 3, 4, and S1). Notably, there are no visible sandy or sandy silt layers within the
366 core sections that are characterized by small changes in sand (SRSD 1-7, 9-14). Instead, the sand
367 is disseminated within the matrix, even within the laminated sections. These small changes in
368 background sand are interpreted to reflect variations in available runoff energy required for the
369 mobilization and transportation of sand into the lake's deepest basin. A depositional model for
370 this process is detailed in Kirby et al. (2010). The glacial sand unit (SRSD 8: 27.6-25.6k cal a
371 BP), however, represents (and requires) an entirely different depositional process and

372 environment. Total sand values during SRSD 8 average $35.4 \% \pm 17.7$, with maximum values
373 exceeding 70 % (Figure 3 and S1). We do not interpret this interval as a period of enhanced run-
374 off. Rather, we suggest (as discussed below) that SRSD 8 reflects a sustained interval of low lake
375 levels (drought) wherein the lake's mud depth boundary, or the depth at which accumulation
376 exceeds erosion, migrated basinward.

377

378 As suggested by the high sand content in SRSD 8, other processes can govern the amount of
379 coarse sediment content in lake basins. For example, the gradual lakeward progradation or
380 landward retreat of the mud depth boundary in response to gradual and sustained lake level
381 regressions or transgressions, respectively, can produce dramatic changes in coarse sediment
382 content over time (Dearing, 1997; Pribyl and Shuman, 2014; Shuman and Serravezza, 2017). In
383 other words, as lake level progressively drops, the mud depth boundary migrates basinward. The
384 result of this migration is a progressive coarsening of sediment basinward. Sediments above the
385 mud depth boundary are typically both visually and analytically different than sediments below
386 the mud depth boundary (Shuman, 2003; Anderson et al., 2001, 2008; Shuman et al., 2009).
387 Therefore, it is possible to determine the sediment's depositional environment – deep lake or
388 shallow lake – using standard sedimentological analyses, such as grain size distributions.
389 Moreover, if these sediment data are coupled with additional climate indicators (such as pollen),
390 the interpretation becomes more robust.

391

392 To explore the differences between sediment type and depositional environment, first we
393 examined the modern relationship between lake water depth and sand content (Figure 5). As
394 expected, sand content decreases with increasing depth. This relationship between lake depth and
395 sediment size is well known and largely a product of sediment focusing and wave energy
396 dissipation with increasing depth (Davis and Ford, 1982; Hilton, 1985; Blais and Kalff, 1995;
397 Anderson et al., 2001, 2008; Shuman et al., 2009). For modern Lake Elsinore, we can estimate
398 the mud depth based on where the asymptote flattens on the y-axis (see Figure 5) (Rowan et al.,
399 1992; Anderson et al., 2008). The data show that the mud depth is approximately 7.3 m with an
400 upper and lower estimate of 6.0 m and 7.8 m, respectively (Figure 5). Second, we compare the
401 grain size distribution between modern sediments below the Lake Elsinore mud depth boundary
402 (6.01-7.32 m) and the SRSD intervals (1-7, 9-14), or the intervals characterized by small changes

403 in percent total sand (Figure 4 and 6). Third, we compare modern Lake Elsinore beach sediment
404 to the glacial sand unit, SRSD 8 (Figure 6).

405
406 These comparisons show that the SRSD intervals 1-7 and 9-14 are similar to the modern grain
407 size distribution found today in Lake Elsinore, for sediments deeper than the mud depth
408 boundary (Figure 6). Conversely, the modern Lake Elsinore beach grain size distribution is more
409 similar to SRSD 8. Taken together, these data suggest that the depositional environment (and
410 processes) for SRSD intervals 1-7 and 9-14 are similar to those governing sedimentation in
411 modern Lake Elsinore below the mud depth boundary (deep lake). SRSD 8, however, is more
412 akin to the depositional environment (and processes) governing sedimentation in modern Lake
413 Elsinore above the mud depth boundary (shallow lake).

414
415 In conclusion, we contend that SRSD intervals 1-7 and 9-14 represent changes in precipitation-
416 related runoff dynamics, resulting in small changes (generally < 15-20 %) in ambient, or
417 background, sand content. This conclusion fits with that observed in modern Lake Elsinore over
418 the 20th century as well as modern river process studies (Inman and Jenkins, 1999; Farnsworth
419 and Milliman, 2003; Warrick and Mertes, 2009; Covault et al., 2010; Kirby et al., 2010, 2014;
420 Xu et al., 2010; Warrick and Barnard, 2012; Gray et al., 2014; Warrick et al., 2015). We argue
421 that it is less likely that these small changes in sand reflect the rapid migration of mud-depth
422 boundary. In fact, over the 20th century, Lake Elsinore lake level and percent total sand show a
423 positive correlation, the exact opposite of that expected if the sand reflected the rapid migration
424 of the mud-depth boundary (Kirby et al., 2010).

425
426 As an additional and independent assessment of this runoff versus mud depth explanation, we
427 compare the sand content in Lake Elsinore between the Holocene and glacial. Sand content in the
428 Holocene record is very low (avg. 3.3 %), much lower on average than at almost any time in the
429 glacial (Figure 4) (Kirby et al., 2010, 2013, this paper). It is known that the Holocene was drier
430 than the glacial in the pswUS (King, 1976; Heusser, 1978; Enzel et al., 1992; Mensing, 2001;
431 Wells et al., 2003; Anderson et al., 2010; Kirby et al., 2013). If we can assume that average lake
432 depth also decreased in the Holocene in response to this change to a drier climate state, we might
433 expect to see an increase in sand as the mud depth boundary migrated basinward. Conversely, if

434 we assume the glacial was wetter and lake levels were generally higher than today (as research
435 suggests), we should see a decrease in sand content as the mud depth boundary migrates away
436 from the basin. In fact, we observe the exact opposite for the both the Holocene (less sand) and
437 the glacial (more sand). Therefore, we argue that the small changes in ambient, or background,
438 sand content between the Holocene and glacial predominantly reflect changes in precipitation-
439 related runoff (drier Holocene = less runoff and wetter glacial = more runoff).

440

441 What about SRSD 8? The grain size distribution as well as total sand content SRSD 8 are clearly
442 different than SRSD 1-7 and 9-14, or the modern sediments below the mud depth boundary
443 (Figure 6). However, the distribution of sediment is quite similar to modern Lake Elsinore beach
444 sediment, or sediment above the mud depth boundary. Consequently, we conclude that SRSD 8
445 reflects a unique sedimentary response to prolonged and sustained glacial drying, during which
446 the mud depth boundary prograded basinward causing the progressive coarsening of sediment.
447 More details pertaining to SRSD 8 are discussed below.

448

449 *Pollen as an ecological tracer*

450

451 The pollen data from core LEDC10-1 were originally reported and interpreted by Heusser et al.
452 (2015). Here, we revisit the pollen data, adding the sediment data, specifically grain size, for a
453 more complete evaluation of the hydrologic-ecologic system (Figure 8). Importantly, because
454 both the pollen and the sediment data were extracted from the same core using the same
455 chronology, we can exam the relationships between hydrologic and ecologic indicators (Hughen
456 et al. 2004; Jennerjahn et al., 2004).

457

458 For this study, we plot the same five pollen types as determined by Principal Component
459 Analysis in Heusser et al. (2015) as reflecting the dominant and most straightforward ecological
460 interpretations. These pollen types include: Amaranthaceae, Asteraceae, Quercus, Pinus, and
461 Juniperus-type (Cupressaceae) (Figure 8). To this five, we add Cyperaceae. Changes in
462 Cyperaceae, Amaranthaceae, and Asteraceae likely reflect vegetation growing within the lake's
463 immediate vicinity. Specifically, they are interpreted to reflect changes in extent of the lake's
464 littoral zone and/or herbaceous and halophytic/semi-arid scrub vegetation. For example, higher

465 values of these three pollen types reflect an expanded littoral zone and an increase in herbaceous
466 and halophytic/semi-arid scrub vegetation, fitting with a shallower lake during a drier climate.
467 Lower values of these pollen reflect a deeper lake during a wetter climate (Figure 8).

468
469 To characterize the vegetation beyond the lake's immediate vicinity, we focus on three tree
470 genera including *Quercus*, *Pinus*, and *Juniperus*-type (*Cupressaceae*). In general, lower values of
471 *Quercus* and higher values of *Pinus* and *Juniperus*-type (*Cupressaceae*) suggest wetter and/or
472 colder conditions. Digging deeper into the tree pollen data and asking the question, "Does a
473 certain genus reflect temperature or moisture more prominently than another," we compared the
474 sand data (i.e., a wetness indicator) to the two dominant and most variable tree genera found in
475 the glacial record: *Pinus* and *Juniperus*-type (*Cupressaceae*) (Figure 8). This simple comparison
476 shows that the sand and *Pinus* data change similarly over centennial to millennial timescales,
477 except where they diverge strongly in the Holocene (SRSD 1: 12.8-10.1k cal a BP). Based on
478 this similarity, we suggest that glacial *Pinus* predominantly reflects changes in moisture
479 availability, like the sand data. *Juniperus*-type (*Cupressaceae*), however, diverges on several
480 occasions from both the sand and *Pinus* data (Figure 8). As a result, we suggest that the
481 *Juniperus*-type (*Cupressaceae*) data reflect a more complex response to temperature and moisture
482 than the *Pinus*, perhaps reflecting *Juniperus*-type's (*Cupressaceae*) resistance to drought stress
483 (Willson et al., 2008). The divergence of the *Juniperus*-type (*Cupressaceae*) pollen from the
484 moisture sensitive *Pinus* and sand suggest that temperature may be more important to controlling
485 the abundance of *Juniperus*-type (*Cupressaceae*) than moisture during the glacial. Albeit a simple
486 interpretation, this compartmentalization of the *Pinus* and *Juniperus*-type (*Cupressaceae*) into
487 moisture and temperature indicators, respectively, allows us to examine relative changes in
488 moisture (sand and *Pinus*) and temperature (*Juniperus*-type) through time.

489
490 Below, the Lake Elsinore record is discussed from oldest to youngest in the context of the SRSD
491 intervals. The paper is not meant to serve as a comprehensive regional site-to-site comparison,
492 such as that from Kirby et al. (2013), Ibarra et al. (2014), Reheis et al. (2015), or Rosenthal et al.
493 (2017). Rather than repeat that information here, we aim to present the complete 32-10k cal a BP
494 Elsinore sediment and pollen data as they inform on the local history of pluvials, droughts, and

495 vegetation in the pswUS. The only exception to this site-specific focus is a brief regional
496 comparison for the glacial sand interval (SRSD 8, 27.6-25.7k cal a BP).

497

498 *MIS 3/2 transition: an unsettled climate regime (SRSD 14-7: 32.3-24.9k cal a BP)*

499

500 The longest period of large amplitude, sustained hydrologic and ecologic variability in the record
501 occurs between SRSD 14-7 (Figure 3, 4, and 8). This period encompasses the MIS 3/2 transition
502 at ca. 29k cal a BP. Sedimentologically, these intervals are characterized by a variety of sediment
503 types, ranging from massive sands (SRSD 8) to discontinuously-laminated sediments with large
504 black organic-rich blebs (Figure 3). Magnetic susceptibility is highly variable as well, indicating
505 changes in sediment provenance, changes in the flux of magnetic minerals into the basin, and/or
506 changes in the preservation of magnetic minerals. Except for a brief interval between 31-30.4k
507 cal a BP, total organic matter is uniformly low, suggesting limited primary productivity and/or
508 poor organic matter preservation. The absence of discrete organic materials for radiocarbon
509 dating throughout most of these intervals supports the latter interpretation. Total carbonate is at
510 or near the lower limit of reliable detection (~4 %) for these intervals (Dean, 1974), suggesting
511 either a lack of carbonate production or carbonate preservation. The pollen data indicate a highly
512 dynamic ecologic system characterized by changes in aquatic littoral zone and herbaceous and
513 halophytic/semi-arid scrub vegetation (Figure 8). Together, these pollen data suggest lake
514 surface contractions and expansions. At the same time, the sand data show considerable large
515 amplitude variability, suggesting changes in winter precipitation related runoff (Figure 8).
516 Within this unsettled climate regime, SRSD 14 (32.3-30.6k cal a BP), 9 (28.4-27.6k cal a BP),
517 and SRSD 8 stand out. SRSD 8 is discussed separately below. SRSD 14 and 9 are interpreted to
518 represent intervals of diminished runoff (low sand), less available moisture (reduced Pinus), and
519 colder conditions (abundant Juniperus-type (Cupressaceae)). Taken together, we interpret SRSD
520 14 and 9 as cold but dry climate intervals. Small increases in Cyperaceae and herbaceous
521 vegetation suggest an increase in the aerial extent of the littoral zone during SRSD 14 and 9, as
522 expected during a drier climate.

523

524 *A closer look at the SRSD 8 (27.6-25.7k cal a BP): a glacial mega-drought?*

525

526 The pollen data indicate a fundamental change in the lake's watershed ecology during SRSD 8
527 (Figure 8) (Heusser et al., 2015). *Pinus* decreased while *Quercus* shows a small increase, together
528 indicating less total moisture. *Juniperus*-type (Cupressaceae) also decreased interpreted to reflect
529 warmer conditions, perhaps characterized by more evaporation and/or less available soil
530 moisture. The aquatic and herbaceous and halophytic/semi-arid scrub vegetation (Cyperaceae,
531 Amaranthaceae, and Asteraceae) thrived suggesting a significant contraction of the lake's surface
532 area while simultaneously increasing the breadth of the littoral zone. These observations resulted
533 in the glacial mega-drought hypothesis proposed by Heusser et al. (2015). At the same time, the
534 lake basin's sedimentology changed substantially with a significant increase in total sand content
535 (Figure 8). Combining the pollen and sediment data, we interpret SRSD 8 as reflecting a
536 prolonged period of drier-than-average climate. This long term drying allowed the gradual, but
537 sustained progradation of coarse sediment found above the mud depth boundary to migrate
538 basinward. The result is a coarse-grained sediment unit similar to modern Lake Elsinore beach
539 sediment (Figure 6).

540
541 This conclusion begs the question, "How shallow was Lake Elsinore during this glacial mega-
542 drought? And, Did the lake desiccate?" Interestingly, there is no evidence for desiccation during
543 SRSD 8, either in the form of mud cracks, root casts, or erosional surfaces. So, if the lake did not
544 desiccate, can we estimate its paleo depth? To answer this question, we explored the modern
545 relationship between lake water depth and grain size distribution, specifically sand content
546 (Figure 5). As expected, sand content decreases with increasing lake water depth. As discussed
547 above, the modern mud depth in Lake Elsinore is approximately 7.3 m with an upper and lower
548 estimate of 6.0 m and 7.8 m, respectively (Figure 5). This estimation does not rule out a much
549 deeper lake, especially during pluvials; it merely provides an upper boundary on minimum lake
550 depth at any given point in time. Using the same sand-depth relationship, we can also estimate
551 the depth during SRSD 8. Averaging the depth and range for percent total sand during SRSD 8
552 provides an average depth estimation of 3.7 m with an upper boundary of 3.2 m and a lower
553 boundary of 4.5 m (Figure 5), clearly above the modern mud depth boundary.

554
555 Using this modern lake water depth-sand relationship, we conclude that Lake Elsinore likely
556 remained a shallow, perennial lake throughout the duration of the glacial mega-drought, despite

557 evidence for a large decrease in available moisture as per the pollen data. The transition to peak
558 sand percent during SRSD 8 is also gradual, suggesting that a progressive and/or sustained
559 drying allowed the gradual, but persistent progradation of mud depth boundary into the deeper
560 lake environment. Finally, the combined sand and pollen data during SRSD 8 indicate that this
561 ~2000-year glacial mega-drought was more severe than other identified glacial droughts in our
562 record, such as SRSD 9 and 14. In the following section, we explore whether or not this nearly
563 ~2000-year glacial mega-drought was regionally pervasive or simply a localized phenomenon?
564

565 *Glacial mega-drought regional comparisons*

566

567 Well-dated, continuous, high-resolution terrestrial records spanning MIS 3 and 2 are relatively
568 uncommon in the pswUS. However, there are two records with adequate dating, resolution, and
569 proxy sensitivity that we will examine in the context of the Elsinore glacial mega-drought (SRSD
570 8): Baldwin Lake (Glover, 2016; Glover et al., 2017) and Lake Manix (Reheis et al., 2015)
571 (Figure 1).
572

573 Baldwin Lake in the San Bernardino Mountains (84km northeast of Elsinore and 1680 m higher
574 elevation) contains a 125k cal a BP record (Glover et al., 2017). Pollen data from Baldwin Lake
575 show an increase in xeric flora approximately coeval to the glacial mega-drought inferred at
576 Elsinore (Glover, 2016). This result indicates a similar ecological response to the drought across
577 elevational gradients within the immediate vicinity of the study site.
578

579 180 km northeast of Elsinore is a well-dated, continuous record of lake elevation for Lake Manix
580 spanning 45-25k cal a BP (Reheis et al., 2015). Although seemingly distal to Elsinore, Lake
581 Manix was fed by the Mojave River, which drains the San Bernardino Mountains, in which
582 Baldwin Lake is located (Figure 1). These mountains are located <50 km north of the San Jacinto
583 Mountains, the predominant water source for Lake Elsinore. Consequently, it is reasonable to
584 expect that both Lake Elsinore and Lake Manix record similar hydroclimatic signals, despite
585 their large physical separation (Figure 1). The major difference between the two archives is that
586 Lake Manix was located within the heart of the Mojave Desert. Although its source was
587 predominantly the high elevation San Bernardino's, the Mojave River (the major influent to Lake

588 Manix) was required to traverse the arid and highly evaporative Mojave Desert. Consequently,
589 transmission of the high elevation hydroclimatic signal from source-to-sink may have
590 experienced more evaporative attenuation than for Lake Elsinore, even under colder (less
591 evaporative) glacial conditions (Enzel, 1992). Recognizing this potential caveat, we compare our
592 results to the Lake Manix lake elevation reconstruction (Figure 8).

593

594 The temporal relationship between the Lake Manix lake elevation reconstruction and the Lake
595 Elsinore hydrologic and ecologic data is intriguing (Figure 8). Considering age control issues
596 (see below) both for Elsinore and Manix, we contend that the Manix lowstand between
597 highstands P6 and P7 correlates to the Elsinore glacial mega-drought (SRSD 8). There is an age
598 offset between the two sites; however, age control issues might explain this discrepancy. First,
599 age control points for Lake Elsinore are absent between 30.7 and 26.5k cal a BP, due to a lack of
600 discrete organic materials (Figure 3), thus our attempt at IRSL dating. Consequently, age control
601 for this interval is based entirely on the age model for Lake Elsinore. Second, as Reheis et al.
602 (2015) acknowledges, most age control for Lake Manix is based on biogenic carbonate from
603 bivalves or gastropods. The reservoir age for Lake Manix likely varied through time, particularly
604 between the Holocene and glacial. However, Reheis et al. (2015) use a standard reservoir
605 correction of 140 years as determined by Owen et al. (2007) and Miller et al. (2010) using late
606 Holocene paired shell-charcoal ages. As a result, the aquatic fauna based carbon dates used by
607 Reheis et al. (2015) for the glacial are likely different than reported due to an unknown glacial
608 reservoir effect. Together, these two site age limitations provide some flexibility in the
609 correlation between the two sites. Because the two sites reflect similar high elevation coastal
610 moisture sources, we argue that it is likely that the two records reflect the same hydroclimatic
611 phenomenon. Alternatively, some of this temporal offset may represent differences caused by
612 varying signal transmission between the much larger, evaporative Lake Manix and the much
613 smaller Lake Elsinore. Either way, we contend that there is regional evidence in the pswUS
614 experienced a nearly 2000-year glacial mega-drought during the early part of MIS 2.

615

616 Certainly, the discovery of a 2000-yr mega-drought in the middle of the last glacial is cause for
617 discussion. Do these glacial mega-droughts characterize the entire glacial? What ocean-
618 atmosphere conditions are required to create such as sustained period of aridity? What do these

619 conditions tell us about climate change and/or non-linear responses to forcings? How are the
620 conditions required for glacial mega-droughts the same or different than the mega-droughts of
621 Holocene? Finally, how will these conditions be modulated by present global warming? There
622 remains much work to characterize and explain the occurrence of mega-droughts during the last
623 glacial.

624

625 *The Last Glacial Maximum (LGM) (SRSDs 7-5, 25.7-19.7k cal a BP)*

626

627 According to Clark et al. (2012), the global LGM is between 26.5-19k cal a BP. Regionally, the
628 LGM may or may not encompass the entirety, or any, of this interval, depending on how one
629 defines the local LGM (LLGM). In the western United States, for example, there is considerable
630 age range variability for the LLGM depending on the climate archive used (e.g., moraines vs.
631 lake sediments vs. marine sediments) (Laabs et al., 2013; Licciardi and Pierce, 2008; Lyle et al.,
632 2012; Menking et al., 2004; Munroe and Laabs, 2013; Munroe et al., 2006; Pak et al., 2012;
633 Rood et al., 2011; Thackray, 2008). Often, for modelling purposes, the LGM is generally defined
634 (and reported) as a singular time slice centered on 21ka, which makes it difficult to compare to
635 time series data (Chiang et al., 2003; Braconnot et al., 2007; Oster et al., 2015; Lora et al., 2017).
636 For Lake Elsinore, we focus on SRSDs 7-5 as the LGM interval. Ostensibly, this determination
637 is somewhat arbitrary. Our rationale, however, for selecting this time interval was to choose an
638 interval that: 1) falls within the timing of the global LGM; 2) is not biased by what we expect to
639 find (e.g., cold and wet); and, 3) does not include the SRSD 8 glacial mega drought interval.

640

641 Using these criteria, the LGM encompasses an interval characterized by variable sedimentology,
642 variable run-off, and variable-to-stable vegetation (Figure 3 and 8). The sedimentology includes:
643 1) massive clay-rich sediment (SRSD 7: 25.7-24.9k cal a BP); 2) variable thickness laminated
644 sediments with large black organic-rich blebs (older half of SRSD 6: 24.9-23.3k cal a BP); 3)
645 discontinuously-laminated organic-rich sediments (younger half of SRSD 6 and the very
646 beginning of SRSD 5); and, 4) variably thick laminated sediments (SRSD 5: 23.3-19.7k cal a
647 BP) (Figure 3). Magnetic susceptibility is variable, indicating changes in sediment provenance,
648 changes in the flux of magnetic minerals into the basin, and/or changes in the preservation of
649 magnetic minerals. Total organic matter is uniformly low except between 25.2-22.9k cal a BP,

650 correlative to the large black organic-rich blebs unit and subsequent discontinuously-laminated
651 unit. Total carbonate increases slightly during the same interval of higher organic matter,
652 suggesting a possible productivity link or an increase in the flux of terrestrial organic detritus.
653 Sand content is higher during SRSD 7 and 6 than during SRSD 5, suggesting a change from
654 more to less runoff throughout the LGM. However, the presence of laminae, even discontinuous
655 laminae, (except during SRSD 7) suggest a deeper, stable lake wherein the core location was
656 below the mud depth boundary and/or the hypolimnion was anoxic. Asteraceae and
657 Amaranthaceae are uniformly low during SRSD 7-5, indicating reduced herbaceous and
658 halophytic/semi-arid scrub vegetation, particularly by comparison to the preceding dry SRSD 8
659 interval. Together, the pollen data suggest a deeper, stable lake as well. Cyperaceae, however,
660 show a decrease from SRSD 7 through 6, before stabilizing at low values in SRSD 5. The
661 Cyperaceae results suggest a gradual reduction in the extent of the lake's littoral zone from
662 SRSD 7 to 6, culminating in a stable, deep lake by SRSD 5. Quercus and Pinus are relatively
663 invariant throughout SRSDs 7-5 and indicate generally wet conditions. Juniperus-type
664 (Cupressaceae) increase from SRSD 7 through 6 and then stabilize during SRSD 5, suggesting a
665 change from a warmer to cooler climate.

666
667 Although the LGM is presented here as encompassing three SRSD intervals, it is only during
668 SRSD 5 that, taken together, the sediment and pollen data obtain relative stability for a 3000-
669 year period. As a result, we suggest that SRSD 5 represent peak LGM conditions locally, or the
670 LLGM. The sediment and vegetation data, however, suggest somewhat contradictory
671 information during SRSD 5. The sand data suggest less runoff during SRSD 5 and thus a drier
672 climate. We note that although the sand content is low, it is still higher than the Holocene
673 average, indicating wetter-than-Holocene conditions. The sedimentology (i.e., variably
674 laminated) also indicates a deep, stable lake wherein the core location was below the mud depth
675 boundary and/or experienced persistent anoxia. The vegetation data, on the other hand, show
676 little to no variability and suggest a perennial lake with a reduced littoral zone and less
677 herbaceous and halophytic/semi-arid scrub vegetation – conditions associated with a wet climate
678 (Figure 8). Notably, the Juniperus-type (Cupressaceae) indicate peak cooling during SRSD 5.
679

680 Combining these results, we suggest that SRSD 5 was wet, as compared to the Holocene and
681 SRSD 8, but less wet than during the subsequent SRSD intervals 4 and 3 (see below and Kirby et
682 al., 2013). Consequently, total winter precipitation runoff diminished as per the decrease in sand
683 content. However, the proliferation and stability of mesic vegetation during an apparently drier
684 LLGM may reflect the LLGM's colder climate (as per the Juniperus-type (Cupressaceae) data)
685 rather than wetter. A colder climate could sustain and promote mesic vegetation, even under
686 conditions of less moisture, if – for example – soil moisture is retained in response to cooler, less
687 evaporative conditions. Cooler, less evaporative conditions may also favor the preservation of a
688 deep lake, even during a period of reduced total precipitation and runoff. In fact, the role cooler
689 glacial temperatures and reduced evaporation played in the development and permanence of
690 large glacial lakes in presently arid environments (e.g. the US Great Basin) is well known (*cf.*
691 Ibarra et al., 2014). This cooler, less evaporative and “drier” LLGM scenario is presented as a
692 possible resolution to this apparent conflict between the sedimentology and the pollen during
693 SRSD 5. Additional, well-dated, and continuous regional records encompassing these intervals
694 are required to evaluate this LLGM hypothesis.

695

696 *Late glacial (SRSD 4 & 3: 19.7-14.4k cal a BP) (Kirby et al., 2013)*

697

698 Using the sand/runoff interpretation, intervals 4 and 3 represent the longest period of greater
699 precipitation-related runoff intensity and/or storm duration observed between 32-10k cal a BP
700 (Figure 4 and 8). As previously noted in Kirby et al. (2013), these intervals encapsulate Heinrich
701 stadial-1 (19-16k cal a BP), a generally cooler period in the Northern Hemisphere (Kindler et al.,
702 2014). In general, the pollen data agree with the runoff indicators, suggesting the presence of a
703 perennial lake with a reduced littoral zone (less Cyperaceae) and less herbaceous and
704 halophytic/semi-arid scrub vegetation (less Amaranthaceae and Asteraceae). The tree pollen data
705 (less Quercus, more Pinus, more Juniperus-type (Cupressaceae)) also indicate a wetter and cooler
706 period. A closer look at the data show that sand increases slightly from the beginning of SRSD 4
707 (19.7-18.2k cal a BP), peaking during the latter half of SRSD 3 (18.2-14.4k cal a BP); the same
708 is true for Pinus. Together, these data suggest a trend towards wetter conditions from SRSD 4 to
709 3. Our temperature indicator, Juniperus-type (Cupressaceae), also suggest a long-term trend from
710 cooler to warmer at the beginning of SRSD 4 through SRSD 3.

711
712 *Late glacial to Holocene transition including the Younger Dryas chronozone (SRSD 2-1: 14.4-*
713 *10.1k cal a BP) (Kirby et al., 2013)*
714
715 The late glacial to Holocene transition features prominently as a period of large hydrologic and
716 ecologic variability (Figure 8). Kirby et al. (2013) details the proposed forcings driving with
717 these changes (i.e., ice sheet extent, AMOC variability, and changing greenhouse gas
718 concentrations); the details are not repeated here. Sand decreases at the SRSD 3/2 transition
719 (14.4k cal a BP) suggesting a reduction in precipitation related runoff. At the same time, there
720 are decreases in Pinus (drier), Quercus (drier), and Juniperus-type (Cupressaceae) (warmer).
721 Asteraceae and Amaranthaceae increase slightly suggesting an expansion of herbaceous and
722 halophytic/semi-arid scrub vegetation. Finally, Cyperaceae increase as well indicating an
723 expansion of the lake's littoral zone. Taken together, these data indicate a climatic drying and
724 warming from SRSD 3 to SRSD 2 (14.4-12.8k cal a BP) (Figure 8). The transition from SRSD 2
725 to SRSD 1 (12.8-10.1k cal a BP) is more complex. Sand decreases suggesting yet another
726 reduction in precipitation related runoff. However, there is an increase in Pinus (wetter) and
727 Quercus (wetter) at the same time, lasting about 600 years. Juniperus-type (Cupressaceae)
728 decrease about 200 years before the sand decrease, suggesting near Holocene temperatures by
729 13.2k cal a BP. Asteraceae and Amaranthaceae generally increase suggesting an additional
730 expansion of herbaceous and halophytic/semi-arid scrub vegetation; although, a brief decrease in
731 Asteraceae correlative to the Pinus increase ca. 13-12.4k cal a BP suggests a possible short-lived
732 lake expansion. Finally, Cyperaceae show no significant change from SRSD 2 to 1, suggesting a
733 stable littoral zone. Taken together, the sediment and vegetation data indicate a complex
734 response at the SRSD 2 to 1 transition (Figure 8). The sedimentology suggests a continued
735 drying trend; whereas, some of the vegetation data (Pinus, Quercus, and Asteraceae) indicate a
736 brief return (~600 years) to wetter and/or cooler conditions. By 12.6-12.4k cal a BP, the data all
737 agree that the climate achieved near Holocene conditions, characterized by drier and warmer
738 climate and a smaller, shallower but stable lake (Figure 8).

739
740

741 **Conclusion**

742

743 In this paper, we present a history of pluvials, droughts, and vegetation in the pswUS spanning
744 32-10k cal a BP. Increases in percent total sand are interpreted to reflect greater precipitation-
745 related runoff (i.e., intensity and/or storm duration) and vice versa. Although the sand data
746 indicate a range of hydroclimatic variability, the late Wisconsin was wetter than the Holocene, in
747 general. Vegetation, as inferred from pollen, reveal generally wetter and cooler conditions during
748 the late Wisconsin as well. The pollen data also indicate intervals of highly variable ecologic
749 change as well as long intervals of vegetative stability. The interval between 32.3-24.9k cal a BP
750 is the longest period of large amplitude, sustained hydrologic and ecologic variability in the
751 record. Punctuating this interval is a proposed glacial mega-drought (27.6-25.7k cal a BP),
752 wherein Lake Elsinore's surface area and depth diminished extensively and mesic flora declined
753 to near Holocene levels. Although the lake did not desiccate during this interval, lake water
754 depth decreased to ~3.2-4.5 m. A lack of desiccation during this extended glacial mega-drought
755 likely reflects cooler temperatures and a decrease in net annual evaporation, thus maintaining a
756 shallow lake under drier conditions. Under similar conditions in the Holocene, the lake would
757 likely desiccate completely. Coeval increases in xeric vegetation at Baldwin Lake in the San
758 Bernardino Mountains (Glover, 2016; Glover et al., 2017) and a large lake level regression at
759 Lake Manix (Mojave Desert) (Reheis et al., 2015) indicates a coherent regional response and
760 shared climatic forcing. We suggest that the LLGM occurred between 23.3-19.7k cal a BP
761 (SRSD 5) encapsulating a nearly 3000-year interval of relative ecologic and hydrologic stability.
762 We interpret the LLGM as a cooler, less evaporative, and "drier" climate; although, the LLGM
763 was not drier than the Holocene but not as wet as the subsequent intervals SRSD 4 & 3 (19.7-
764 14.4k cal a BP). SRSD intervals 4 and 3 represent the longest period of greater precipitation-
765 related runoff intensity and/or storm duration observed between 32-10k cal a BP. There is
766 evidence for a trend toward wetter and warmer conditions beginning at 19.7k cal a BP and
767 peaking at 14.4k cal a BP. The late glacial to Holocene transition (SRSD 2-1: 14.4-10.1k cal a
768 BP) features prominently as a period of large hydrologic and ecologic variability. In general,
769 SRSD 2 is characterized as an interval of reduced runoff, a warmer climate, and a decrease in
770 lake surface area and depth. The relationship, however, between the hydrologic and ecologic
771 indicators is more complex during the SRSD 2 to 1 transition. The vegetation data (*Pinus*,
772 *Quercus*, and *Asteraceae*) indicate a brief return (~600 years) to wetter conditions between 13-

773 12.6/12.4k cal a BP; whereas, the hydrologic indicator indicate a continued decrease in runoff.
774 By 12.6-12.4k cal a BP, the ecology and hydrology achieved near Holocene conditions. Future
775 work will examine these results in the context of regional and hemispheric data as well as late
776 Wisconsin climatic forcings.

777

778 **Acknowledgements**

779

780 This research was funded by the National Science Foundation (#031511, #0731843, and
781 #1203549) and the American Chemical Society-Petroleum Research Fund (#4187-B8). Special
782 thanks to Mr. Pat Kilroy and the City of Lake Elsinore for lake access; Mr. Joe Holbrook
783 (CSUF) for help opening the cores; Mr. Peter Cattaneo (Syracuse University) for expert advice
784 and service collecting and processing the seismic reflection data. Most importantly, this work
785 would not be possible without the excellent service and research quality cores collected by Mr.
786 John Gregg and Gregg Drilling and Testing, Inc. The authors thank Mr. Daniel Ibarra, Dr. David
787 Miller, one anonymous reviewer, and the editor (Dr. Joe Liccardi) for thoughtful and helpful
788 reviews. Sandy discussions with Dr. Joe Carlin and comments by Dr. Nicole Bonuso are
789 appreciated, too. MEK dedicates this paper to Dr. John T. Andrews for giving me an opportunity.

790

791

792 **References**

793

794 Anderson M, Whiteaker L, Wakefield E, Amrhein C, 2008. Properties and distribution of
795 sediment in the Salton Sea, California: an assessment of predictive models. *Hydrobiologia* 604,
796 97-110.

797

798 Anderson MA, 2001. Internal loading and nutrient cycling in Lake Elsinore. In. *Lake Elsinore:*
799 *Santa Ana Regional Water Quality Control Board*, 52.

800

801 Anderson, R.S., Starratt, S., Jass, R.M.B., Pinter, N., 2010. Fire and vegetation history on Santa
802 Rosa Island, Channel Islands, and long-term environmental change in southern California.
803 *Journal of Quaternary Science* 25, 782-797.

804
805 Antevs E, 1948. Climatic Changes and Pre-White Man. The Great Basin, with emphasis on
806 glacial and postglacial times. University of Utah Bulletin 38, 166-91.
807
808 Blaauw M, Christen JA, 2011. Flexible paleoclimate age-depth models using an autoregressive
809 gamma process. *Bayesian Analysis* 6, 457-74.
810
811 Blais, J.M., Kalff, J., 1995. The Influence of Lake Morphometry on Sediment Focusing.
812 *Limnology and Oceanography* 40, 582-588.
813
814 Braconnot, P., Otto-Bliesner, B., Harrison, S., Joussaume, S., Peterchmitt, J.Y., Abe-Ouchi, A.,
815 Crucifix, M., Driesschaert, E., Fichefet, T., Hewitt, C.D. and Kageyama, M., 2007. Results of
816 PMIP2 coupled simulations of the Mid-Holocene and Last Glacial Maximum–Part 1:
817 experiments and large-scale features. *Climate of the Past*, 3(2), pp.261-277.
818
819 Brito-Castillo L, Douglas AV, Leyva-Contreras A, Lluich-Belda D, 2003. The effect of large-
820 scale circulation on precipitation and streamflow in the Gulf of California continental watershed.
821 *International Journal of Climatology* 23, 751-68.
822
823 Cayan DR, Peterson DH, 1989. The Influence of North Pacific Atmospheric Circulation on
824 Streamflow in the West in Aspects of Climate Variability in the Pacific and the Western
825 Americas. In: Agu, ed. *Geophysical Monograph Series*. Washington, 375-97. (Union AG, ed.
826 55.)
827
828 Cayan DR, Redmond KT, Riddle RG, 1999. ENSO and hydrologic extremes in the western
829 United States. *Journal of Climate* 12, 2881-93.
830
831 Chiang, J.C., Biasutti, M. and Battisti, D.S., 2003. Sensitivity of the Atlantic intertropical
832 convergence zone to last glacial maximum boundary conditions. *Paleoceanography*, 18(4).
833

834 Clark PU, Shakun JD, Baker PA, et al., 2012. Global climate evolution during the last
835 deglaciation. *Proc Natl Acad Sci U S A* 109, E1134-42.
836

837 Covault J., Romans B., Fildani A, Mcgann M, Graham S., 2010. Rapid Climatic Signal
838 Propagation from Source to Sink in a Southern California Sediment-Routing System. *The*
839 *Journal of Geology* 118, 247-59.
840

841 Csato I, Kendall CGSC, Nairn AEM, Baum GR, 1997. Sequence stratigraphic interpretations in
842 the southern Dead Sea basin, Israel. *Geological Society of America Bulletin* 109, 1485-501.
843

844 Damiata, B.N. and Lee, T.C., 1986. Geothermal exploration in the vicinity of Lake Elsinore,
845 Southern California. *Geothermal Resource Council Trans*, 10, pp.119-123.
846

847 Davis, M.B., Ford, M.S., 1982. Sediment Focusing in Mirror Lake, New Hampshire. *Limnology*
848 *and Oceanography* 27, 137-150.
849

850 Dean, W. E. (1974). Determination of carbonate and organic matter in calcareous sedimentary
851 rocks by loss on ignition: Comparison with other methods. *Journal of Sedimentary Petrology*,
852 44, 242-248.
853

854 Dearing, J.A., 1997. Sedimentary indicators of lake-level changes in the humid temperate zone:
855 A critical review. *Journal of Paleolimnology* 18, 1-14.
856

857 Enzel Y, 1992. Flood Frequency of the Mojave River and the Formation of Late Holocene Playa
858 Lakes, Southern California, USA. *The Holocene* 2, 11-8.
859

860 Enzel, Y., Brown, W.J., Anderson, R.Y., Mcfadden, L.D., Wells, S.G., 1992. Short-Duration
861 Holocene Lakes in the Mojave River Drainage-Basin, Southern California. *Quaternary Research*
862 38, 60-73.
863

864 Enzel Y, Agnon A, Stein M, 2006. *New Frontiers in Dead Sea Paleoenvironmental Research*.
865 Boulder: Geological Society of America.
866

867 Farnsworth, K.L., Milliman, J.D., 2003. Effects of climatic and anthropogenic change on small
868 mountainous rivers: the Salinas River example. *Global and Planetary Change* 39, 53-64.
869

870 Glover, K.C., 2016. *Southern California climate and vegetation over the past 125,000 years from*
871 *lake sequences in the San Bernardino Mountains*. Ph.D. Thesis, University of California - Los
872 Angeles, Los Angeles.
873

874 Glover KC, Macdonald GM, Kirby ME, et al., 2017. Evidence for orbital and North Atlantic
875 climate forcing in alpine Southern California between 125 and 10 ka from multi-proxy analyses
876 of Baldwin Lake. *Quaternary Science Reviews* 167, 47-62.
877

878 Gray AB, Pasternack GB, Watson EB, Warrick JA, Goñi MA, 2015. Effects of antecedent
879 hydrologic conditions, time dependence, and climate cycles on the suspended sediment load of
880 the Salinas River, California. *Journal of Hydrology* 525, 632-49.
881

882 Gray AB, Warrick JA, Pasternack GB, Watson EB, Goñi MA, 2014. Suspended sediment
883 behavior in a coastal dry-summer subtropical catchment: Effects of hydrologic preconditions.
884 *Geomorphology* 214, 485-501.
885

886 Hanson R, Dettinger M, Newhouse M, 2006. Relations between climatic variability and
887 hydrologic time series from four alluvial basins across the southwestern United States.
888 *Hydrogeology Journal* 14, 1122-46.
889

890 Heusser, L., 1978. Pollen in Santa Barbara Basin, California; a 12,000-yr record. *Geological*
891 *Society of America Bulletin* 89, 673-678.
892

893 Heusser L, Sirocko F, 1997. Millennial pulsing of environmental change in southern California
894 from the past 24 k.y: A record of Indo-Pacific ENSO events? *Geology* 25, 243-6.

895
896 Heusser LE, 1995. Pollen stratigraphy and paleoecologic interpretation of the 160-k.y. record
897 from Santa Barbara Basin, Hole 893A. In: Kennett JP, Baldauf JG, Lyle M, eds. Proc. ODP, Sci.
898 Results. College Station, TX, 265-79. (146.)
899
900 Heusser LE, Kirby ME, Nichols JE, 2015. Pollen-based evidence of extreme drought during the
901 last Glacial (32.6–9.0 ka) in coastal southern California. *Quaternary Science Reviews* 126, 242-
902 53.
903
904 Hiner CA, Kirby ME, Bonuso N, Patterson WP, Palermo J, Silveira E, 2016. Late Holocene
905 hydroclimatic variability linked to Pacific forcing: evidence from Abbott Lake, coastal central
906 California. *Journal of Paleolimnology* 56, 299-313.
907
908 Hudson T, 1978. *Lake Elsinore Valley: its story*. Lake Elsinore: Mayhall Print Shop.
909
910 Hughen KA, Eglinton TI, Xu L, Makou M, 2004. Abrupt tropical vegetation response to rapid
911 climate changes. *Science* 304, 1955-9.
912
913 Hull AG, 1990. *Seismotectonics of the Elsinore-Temecula Trough, Elsinore Fault Zone,*
914 *Southern California*. Santa Barbara: UC Santa Barbara, Ph.D.
915
916 Hull AG, Nicholson C, 1992. Seismotectonics of the northern Elsinore fault zone, southern
917 California. *Bulletin of the Seismological Society of America* 82, 800-18.
918
919 Ibarra DE, Egger AE, Weaver KL, Harris CR, Maher K, 2014. Rise and fall of late Pleistocene
920 pluvial lakes in response to reduced evaporation and precipitation: Evidence from Lake Surprise,
921 California. *Geological Society of America Bulletin*, B31014. 1.
922
923 Inman DL, Jenkins SA, 1999. Climate change and the episodicity of sediment flux of small
924 California Rivers. *Journal of Geology* 107, 251-70.
925

926 Jennerjahn TC, Ittekkot V, Arz HW, Behling H, Pätzold J, Wefer G, 2004. Asynchronous
927 terrestrial and marine signals of climate change during Heinrich events. *Science* 306, 2236-9.
928

929 Kam J, Sheffield J, 2016. Increased drought and pluvial risk over California due to changing
930 oceanic conditions. *Journal of Climate* 29, 8269-79.
931

932 Kindler P, Guillevic M, Baumgartner M, Schwander J, Landais A, Leuenberger M, 2014.
933 Temperature reconstruction from 10 to 120 kyr b2k from the NGRIP ice core. *Climate of the*
934 *Past* 10, 887.
935

936 King Jr, T.J., 1976. Late Pleistocene-early Holocene history of coniferous woodlands in the
937 Lucerne Valley region, Mohave Desert, California. *Western North American Naturalist* 36, 227-
938 238.
939

940 Kirby M, Lund S, Anderson M, Bird B, 2007. Insolation forcing of Holocene climate change in
941 Southern California: a sediment study from Lake Elsinore. *Journal of Paleolimnology* 38, 395-
942 417.
943

944 Kirby ME, Feakins SJ, Bonuso N, Fantozzi JM, Hiner CA, 2013. Latest Pleistocene to Holocene
945 hydroclimates from Lake Elsinore, California. *Quaternary Science Reviews* 76, 1-15.
946

947 Kirby ME, Feakins SJ, Hiner CA, et al., 2014. Tropical Pacific forcing of Late-Holocene
948 hydrologic variability in the coastal southwest United States. *Quaternary Science Reviews* 102,
949 27-38.
950

951 Kirby ME, Lund SP, Patterson WP, et al., 2010. A Holocene record of Pacific Decadal
952 Oscillation (PDO)-related hydrologic variability in Southern California (Lake Elsinore, CA).
953 *Journal of Paleolimnology* 44, 819-39.
954

955 Kirby ME, Lund SP, Poulsen CJ, 2005. Hydrologic variability and the onset of modern El Nino-
956 Southern Oscillation: a 19 250-year record from Lake Elsinore, southern California. *Journal of*
957 *Quaternary Science* 20, 239-54.
958

959 Kirby ME, Poulsen CJ, Lund SP, Patterson WP, Reidy L, Hammond DE, 2004. Late Holocene
960 lake-level dynamics inferred from magnetic susceptibility and stable oxygen isotope data: Lake
961 Elsinore, Southern California (USA). *Journal of Paleolimnology* 31, 275-93.
962

963 Krummenacher D, Gastil RG, Bushee J, Doupont J, 1975. K-Ar Apparent Ages, Peninsular
964 Ranges Batholith, Southern California and Baja California. *Geological Society of America*
965 *Bulletin* 86, 760-8.
966

967 Laabs BJC, Munroe JS, Best LC, Caffee MW, 2013. Timing of the last glaciation and subsequent
968 deglaciation in the Ruby Mountains, Great Basin, USA. *Earth and Planetary Science Letters* 361,
969 16-25.
970

971 Licciardi JM, Pierce KL, 2008. Cosmogenic exposure-age chronologies of Pinedale and Bull
972 Lake glaciations in greater Yellowstone and the Teton Range, USA. *Quaternary Science*
973 *Reviews* 27, 814-31.
974

975 Löffverström M, Caballero R, Nilsson J, Kleman J, 2014. Evolution of the large-scale
976 atmospheric circulation in response to changing ice sheets over the last glacial cycle. *Climate of*
977 *the Past* 10, 1453-71.
978

979 Lora, J.M., Mitchell, J.L., Tripathi, A.E., 2016. Abrupt reorganization of North Pacific and
980 western North American climate during the last deglaciation. *Geophysical Research Letters* 43,
981 11796-11804.
982

983 Lora JM, Mitchell JL, Risi C, Tripathi AE, 2017. North Pacific atmospheric rivers and their
984 influence on western North America at the Last Glacial Maximum. *Geophysical Research*
985 *Letters*.

986
987 Lyle M, Heusser L, Ravelo C, et al., 2012. Out of the tropics: the Pacific, Great Basin lakes, and
988 late Pleistocene water cycle in the western United States. *Science* 337, 1629-33.
989
990 Lynch HB, 1931. Rainfall and stream run-off in Southern California since 1769. In. Los Angeles:
991 The Metropolitan Water District of Southern California, 31.
992
993 Mann J, J.F., 1956. The origin of Elsinore Lake Basin. *Bulletin of the Southern California*
994 *Academy of Sciences* 55, 72-8.
995
996 Masi GJ. Orographic and large-scale influence on Southern California precipitation patterns.
997 *Proceedings of the Sixth Conference on Coastal Atmospheric and Oceanic Prediction and*
998 *Processes*, 2005.
999
1000 Menking KM, Syed KH, Allen BD, Anderson RY, Shafike NG, 2004. Wetter or colder during
1001 the Last Glacial Maximum? Revisiting the pluvial lake question in southwestern North America
1002 *Quaternary Research* 62, 280-8.
1003
1004 Mensing, S.A., 2001. Late-Glacial and Early Holocene vegetation and climate change near
1005 Owens Lake, eastern California. *Quaternary Research* 55, 57-65.
1006
1007 Miller, D.M., Schmidt, K.M., Mahan, S.A., McGeehin, J.P., Owen, L.A., Barron, J.A.,
1008 Lehmkuhl, F. and Löhner, R., 2010. Holocene landscape response to seasonality of storms in the
1009 Mojave Desert. *Quaternary International*, 215(1), pp.45-61.
1010
1011 Morton D, Miller F. K/Ar apparent ages of plutonic rocks from the northern part of the
1012 Peninsular Ranges batholith, southern California. *Proceedings of the Geological Society of*
1013 *America Abstracts with Programs*, 1987, 435.
1014

1015 Munroe JS, Laabs BJ, Shakun JD, et al., 2006. Latest Pleistocene advance of alpine glaciers in
1016 the southwestern Uinta Mountains, Utah, USA: evidence for the influence of local moisture
1017 sources. *Geology* 34, 841-4.
1018

1019 Munroe JS, Laabs BJC, 2013. Temporal correspondence between pluvial lake highstands in the
1020 southwestern US and Heinrich Event 1. *Journal of Quaternary Science* 28, 49-58.
1021

1022 Myers N, Mittermeier RA, 2000. Biodiversity hotspots for conservation priorities. (Cover story).
1023 *Nature* 403, 853.
1024

1025 Neelin JD, Langenbrunner B, Meyerson JE, Hall A, Berg N, 2013. California Winter
1026 Precipitation Change under Global Warming in the Coupled Model Intercomparison Project
1027 Phase 5 Ensemble. *Journal of Climate* 26, 6238-56.
1028

1029 Oster JL, Ibarra DE, Winnick MJ, Maher K, 2015. Steering of westerly storms over western
1030 North America at the Last Glacial Maximum. *Nature Geosci* 8, 201-5.
1031

1032 Owen, L.A., Bright, J., Finkel, R.C., Jaiswal, M.K., Kaufman, D.S., Mahan, S., Radtke, U.,
1033 Schneider, J.S., Sharp, W., Singhvi, A.K. and Warren, C.N., 2007. Numerical dating of a Late
1034 Quaternary spit-shoreline complex at the northern end of Silver Lake playa, Mojave Desert,
1035 California: A comparison of the applicability of radiocarbon, luminescence, terrestrial
1036 cosmogenic nuclide, electron spin resonance, U-series and amino acid racemization
1037 methods. *Quaternary International*, 166(1), pp.87-110.
1038

1039 Pak DK, Lea DW, Kennett JP, 2012. Millennial scale changes in sea surface temperature and
1040 ocean circulation in the northeast Pacific, 10–60 kyr BP. *Paleoceanography* 27.
1041

1042 Pribyl, P., Shuman, B.N., 2014. A computational approach to Quaternary lake-level
1043 reconstruction applied in the central Rocky Mountains, Wyoming, USA. *Quaternary Research*
1044 82, 249-259.
1045

1046 Pyke, B. N., 2013. A holocene hydroclimatic investigation of lake elsinore, southern california,
1047 using seismic reflection and sediment core data, MS Thesis, California State University,
1048 Fullerton, 96pp.
1049

1050 Reheis MC, Miller DM, Mcgeehin JP, Redwine JR, Oviatt CG, Bright J, 2015. Directly dated
1051 MIS 3 lake-level record from Lake Manix, Mojave Desert, California, USA. *Quaternary*
1052 *Research* 83, 187-203.
1053

1054 Rhodes EJ, 2015. Dating sediments using potassium feldspar single-grain IRSL: Initial
1055 methodological considerations. *Quaternary International* 362, 14-22.
1056

1057 Rodionov S, 2015. A sequential method of detecting abrupt changes in the correlation coefficient
1058 and its application to Bering Sea climate. *Climate* 3, 474-91.
1059

1060 Rodionov, S.N., 2004. A sequential algorithm for testing climate regime shifts. *Geophysical*
1061 *Research Letters*, 31(9).
1062

1063 Romans BW, Normark WR, Mcgann MM, Covault JA, Graham SA, 2009. Coarse-grained
1064 sediment delivery and distribution in the Holocene Santa Monica Basin, California: implications
1065 for evaluating source-to-sink flux at millennial time scales. *Geological Society of America*
1066 *Bulletin* 121, 1394-408.
1067

1068 Rood DH, Burbank DW, Finkel RC, 2011. Chronology of glaciations in the Sierra Nevada,
1069 California, from ¹⁰Be surface exposure dating. *Quaternary Science Reviews* 30, 646-61.
1070

1071 Rosenthal, J.S., Meyer, J., Palacios-Fest, M.R., Young, D.C., Ugan, A., Byrd, B.F., Gobalet, K.
1072 and Giacomo, J., 2017. Paleohydrology of China Lake basin and the context of early human
1073 occupation in the northwestern Mojave Desert, USA. *Quaternary Science Reviews*, 167, pp.112-
1074 139.
1075

1076 Rowan DJ, Kalff J, Rasmussen JB, 1992. Estimating the Mud Deposition Boundary Depth in
1077 Lakes from Wave Theory. *Canadian Journal of Fisheries and Aquatic Sciences* 49, 2490-7.
1078
1079 Scholz, C.A., 2001. Application of seismic sequence stratigraphy in lacustrine basins, in: Last,
1080 W.M., Smol, J.P. (Eds.), *Tracking Environmental Change Using Lake Sediments*. Kluwer
1081 Academic Publishers, Dordrecht, pp. 7-22.
1082
1083 Seager R, Ting M, Li C, et al., 2013. Projections of declining surface-water availability for the
1084 southwestern United States. *Nature Clim. Change* 3, 482-6.
1085
1086 Shields CA, Kiehl JT, 2016. Atmospheric river landfall-latitude changes in future climate
1087 simulations. *Geophysical Research Letters* 43, 8775-82.
1088
1089 Shuman, B., 2003. Controls on loss-on-ignition variation in cores from two shallow lakes in the
1090 northeastern United States. *Journal of Paleolimnology* 30, 371-385.
1091
1092 Shuman, B., Henderson, A.K., Colman, S.M., Stone, J.R., Fritz, S.C., Stevens, L.R., Power,
1093 M.J., Whitlock, C., 2009. Holocene lake-level trends in the Rocky Mountains, U.S.A.
1094 *Quaternary Science Reviews* 28, 1861-1879.
1095
1096 Shuman, B.N., Serravezza, M., 2017. Patterns of hydroclimatic change in the Rocky Mountains
1097 and surrounding regions since the last glacial maximum. *Quaternary Science Reviews* 173, 58-
1098 77.
1099
1100 Silver L, Taylor Jr H, Chappell B. Some petrological, geochemical and geochronological
1101 observations of the Peninsular Ranges batholith near the international border of the USA and
1102 Mexico, *Mesozoic Crystalline Rocks* PL Abbott, VR Todd, 83–110, Department of Geological
1103 Sciences, San Diego State University, Guideb. for Geol. Proceedings of the Dept. of Geol. Sci.,
1104 Guidebook for Geological Society of America Annual Meeting, San Diego, Calif, 1979.
1105

1106 Thackray GD, 2008. Varied climatic and topographic influences on Late Pleistocene mountain
1107 glaciation in the western United States. *Journal of Quaternary Science* 23, 671-81.
1108
1109 Thiros, S. A. (1781). Section 12. Conceptual understanding and groundwater quality of the
1110 basin-fill aquifers in the Santa Ana Basin, California. *US Geological Survey Professional*
1111 *Paper, 2010*, 219-65.
1112
1113 Topozada TR, Parke DL, Higgins CT, 1978. Seismicity of California, 1900-1931. California
1114 Division of Mines and Geology.
1115
1116 Vaughan PR, Thorup KM, Rockwell TK, 1999. Paleoseismology of the Elsinore fault at Agua
1117 Tibia Mountain, southern California. *Bulletin of the Seismological Society of America* 89, 1447-
1118 57.
1119
1120 Warrick, J.A., Barnard, P.L., 2012. The offshore export of sand during exceptional discharge
1121 from California rivers. *Geology* 40, 787-790.
1122
1123 Warrick JA, Melack JM, Goodridge BM, 2015. Sediment yields from small, steep coastal
1124 watersheds of California. *Journal of Hydrology: Regional Studies* 4, 516-34.
1125
1126 Warrick, J.A., Mertes, L.A.K., 2009. Sediment yield from the tectonically active semiarid
1127 Western Transverse Ranges of California. *Geological Society of America Bulletin* 121, 1054-
1128 1070.
1129
1130 Warrick JA, Mertes LA, Washburn L, Siegel DA, 2004. A conceptual model for river water and
1131 sediment dispersal in the Santa Barbara Channel, California. *Continental Shelf Research* 24,
1132 2029-43.
1133
1134 Warrick JA, Rubin DM, 2007. Suspended-sediment rating curve response to urbanization and
1135 wildfire, Santa Ana River, California. *Journal of Geophysical Research: Earth Surface* 112.
1136

1137 Weber Jr F, 1977. Seismic hazards related to geologic factors, Elsinore and Chino fault zones,
1138 northwestern Riverside County, California, Calif Div. Div. Mines and Geol., Open-File Report,
1139 77-4.

1140

1141 Wells SG, Brown JB, Enzel Y, Anderson RY, Mcfadden LD, eds, 2003. Late Quaternary
1142 geology and paleohydrology of pluvial Lake Mojave, southern California. Boulder, CO:
1143 Geological Society of America.

1144

1145 Willson, C.J., Manos, P.S. and Jackson, R.B., 2008. Hydraulic traits are influenced by
1146 phylogenetic history in the drought-resistant, invasive genus *Juniperus* (Cupressaceae). *American*
1147 *Journal of Botany*, 95(3), pp.299-314.

1148

1149 Wong CI, Potter GL, Montañez IP, Otto-Bliesner BL, Behling P, Oster JL, 2016. Evolution of
1150 moisture transport to the western US during the last deglaciation. *Geophysical Research Letters*
1151 43, 3468-77.

1152

1153 Xu JP, Swarzenski PW, Noble M, Li A-C, 2010. Event-driven sediment flux in Hueneme and
1154 Mugu submarine canyons, southern California. *Marine Geology* 269, 74-88.

1155

1156 Yilmaz, Ö., 2001. *Seismic data analysis: Processing, inversion, and interpretation of seismic*
1157 *data*. Society of exploration geophysicists.

1158

1159 Yoon J-H, Wang SS, Gillies RR, Kravitz B, Hipps L, Rasch PJ, 2015. Increasing water cycle
1160 extremes in California and in relation to ENSO cycle under global warming. *Nature*
1161 *communications* 6.

1162
1163

1164 **Figure Captions**

1165

1166 Figure 1. A) Study site with bathymetry, core locations, and seismic line locations discussed in
1167 the text; B) Regional map with Lake Elsinore and other sites mentioned in the text; C) Seismic

1168 line map. Abbreviations: SJ Mtns = San Jacinto Mountains; SBB = Santa Barbara Basin. Core
1169 references: LESS02-8/10 (Kirby et al., 2004, 2005); LEGC03-2/3 (Kirby et al., 2007, 2010);
1170 LEDC10-1 (Kirby et al., 2013; Heusser et al., 2015; this paper).

1171

1172 Figure 2. A) LEDC10-1 age versus depth, B) and C) Age model differences between this paper
1173 and Kirby et al. (2013) and Heusser et al. (2015).

1174

1175 Figure 3. LEDC10-1 core sediment data. A) Stratigraphic column with enhanced, subjective
1176 coloring to highlight variations, B) Magnetic susceptibility, C) Percent total organic matter (LOI
1177 550 °C), D) Percent total carbonate (LOI 950 °C), E) Percent total sand, silt, and clay, F) Percent
1178 sand without the glacial sand unit. SRSD intervals are highlighted by dashed grey boxes.

1179

1180 Figure 4. Percent total sand with sequential regime shift detection break-points shown by bold
1181 black line. Holocene sand average (3.3 %) from Kirby et al. (2010) is shown as dashed black
1182 line. SRSD intervals are highlighted by dashed grey boxes.

1183

1184 Figure 5. Lake bottom sediment percent sand versus lake water depth. The green dashed lines
1185 represent the 95% bootstrap confidence intervals for the regression curve.

1186

1187 Figure 6. Lake Elsinore grain size distributions plots: 1) modern Lake Elsinore beach sample
1188 (thick blue line); 2) the glacial sand unit SRSD 8 (thick red line); 3) all modern lake bottom
1189 samples between 6.01 and 7.32 m (thin grey lines); and 4) SRSD intervals 1-7 and 9-14 (thin
1190 green line).

1191

1192 Figure 7. Seismic reflection lines A) LE line 33 and B) LE line 10. Line intersections are shown
1193 as well as the position of core LEDC10-1. The black + are processing artifacts.

1194

1195 Figure 8. Sand-pollen plots versus age. Y-axes oriented so that wet and/or cold interpretation is
1196 always up. A) Percent total sand vs. percent Juniperus-type (Cupressaceae), B) Percent total sand
1197 vs. percent Pinus, C) Percent total sand vs. percent Quercus, D) Percent total sand vs. percent
1198 Asteraceae, E) Percent total sand vs. percent Amaranthaceae, and F) Percent total sand vs.

1199 percent Cyperaceae. G) Lake Manix altitude redrawn from Reheis et al. (2015). P5-8 represent
1200 Lake Manix highstands from Reheis et al. (2015). The small blue boxes with horizontal error
1201 lines represent the weighted means of statistical age groups (Reheis et al., 2015). The SRSD
1202 intervals are highlighted as dashed blue boxes. The glacial mega-drought (SRSD 8) is
1203 highlighted by a light-yellow box. The LLGM is highlighted by a light grey box.

1204

1205 **Supplemental Figure Captions**

1206

1207 Figure S1. LEDC10-1 percent sand by size groupings from A) total sand to E) coarse sand. Very
1208 coarse sand (1000-2000 μm) is not shown.

1209

1210 Figure S2. The absolute time step between individual grain size and pollen analyses.

Table 1. Age data for core LEDC10-1

Sample #	LEDC10-1	Depth Range (cm)	Average Depth (cm)	Material	ID	$\delta^{13}\text{C}(\text{‰})^a$	C-14 Age (BP) Used in BACON (v2.2)	\pm	2-Sigma Range	Age (cy BP)
1		1274-1275	1274.5	Gastropods	*N93630	-25	8,655	35	9,541-9,684	9,613
2		1274-1275	1274.5	Gastropods	*N93631	-25	8,710	35	9,548-9,780	9,664
3		1396-1398	1397.0	Bulk	*94679	-25	10,155 (9,450 Res. Corrected #)	46	11,685-12,030	11,858
4		1508-1510	1509.0	Bulk	*94680	-22.9	10,950 (10,240 Res. Corrected #)	46	12,648-12,964	12,806
5		1540-1542	1541.0	Bulk	*94681	-25	11,650 (10,940 Res. Corrected #)	46	13,334-13,691	13,513
6		1618-1620	1619.0	Bulk	*94682	-24.6	12,200 (11,490 Res. Corrected #)	46	13,887-14,202	14,045
7		1683-1685	1684.0	Mixed Discrete	*N95444	-25	12,140	280	13,437-15,067	14,252
8		1710-1711	1710.5	Mixed Discrete	*N95445	-25	12,460	120	14,091-15,090	14,591
9		1723-1725	1724.0	Mixed Discrete (0.035mgC)	^134836	-25	12,190	290	13,470-15,155	14,313
10		1738-1739	1738.5	Mixed Discrete	*N95446	-25	13,420	230	15,390-16,932	16,161
11		1747-1748	1747.5	Charcoal	*N94003	-25	13,260	35	15,578-16,699	16,139
12		1778-1779	1778.5	Wood	*N94004	-25	13,775	35	16,734-17,049	16,892
13		1823-1824	1823.5	Charcoal	*N94005	-25	14,360	30	17,154-17,790	17,472
14		1823-1824	1823.5	Charcoal	*N94243	-25	14,310	30	17,082-17,706	17,394
15		1870-1872	1871.0	Charcoal; Charred Grass (0.073mgC)	^134837	-25	14,740	200	17,460-18,424	17,942
16		1997-1999	1998.0	Seeds	*N94006	-25	16,580	40	19,461-19,936	19,699
17		2019-2020	2019.5	Seeds	*N94007	-25	16,880	40	19,832-20,321	20,077
18		2081-2082	2081.5	Wood	*N94008	-25	17,980	180	20,911-22,128	21,520
19		2198-2199	2198.5	Seeds	*N94010	-25	19,630	40	23,134-23,779	23,457
20		2280-2282	2281.0	Small Twig	^134839	-23.4	20,870	90	24,881-25,516	25,199
21		2292-2293	2292.5	Charcoal	^134840	-24.1	21,370	90	25,510-25,899	25,700
22		2344-2345	2344.5	Charcoal	*N94245	-25	21,025	40	24,940-25,556	25,248
23		2344-2345	2344.5	Charcoal	*N94011	-25	21,120	70	24,834-25,494	25,164
24		2384-2386	2385.0	Charcoal	^118908	-25	22,010	80	26,078-26,843	26,460
25		2425-2427	2426.0	Small Charcoal (0.16mgC)	^134841	-23.9	21,760	210	25,650-26,481	26,061
26	2438-2453	2445.5		IRSL method	UCLA	na	29,200 α	2,000	na	
27	2500-2517	2508.5		IRSL method	UCLA	na	31,300 α	2,200	na	
28		2830-2832	2831.0	Charcoal	^118909	-25	25,940	110	30,419-31,016	30,720
29		2860-2861	2860.5	Wood	*150331	-25	26,550	90	30,970-31,262	31,116
30		2860-2861	2860.5	Wood	*150337	-25	26,270	80	30,758-31,179	30,969

^a $\delta^{13}\text{C}$ values are the assumed values according to Stuiver and Polach (1977) when given without decimal places.

^a $\delta^{13}\text{C}$ values measured for the material itself are given with a single decimal place.

^b CALIB 6.0.1 Program (Stuiver and Reimer, 1986)

* LLNL AMS Results

^ UCI AMS Results

Correction based on paired bulk - discrete samples - see Kirby et al. (2013)

α Not used in the age model

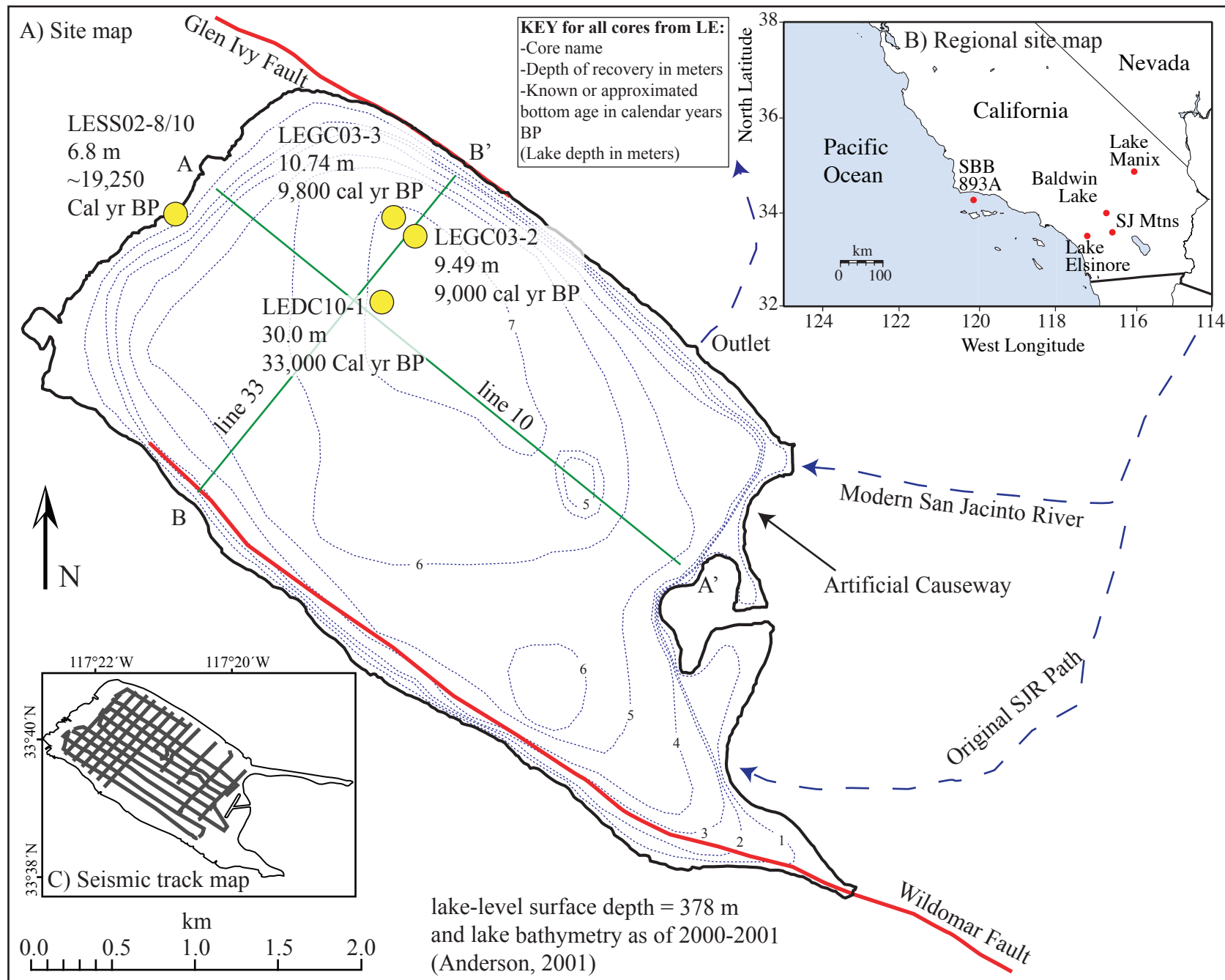


Figure 1

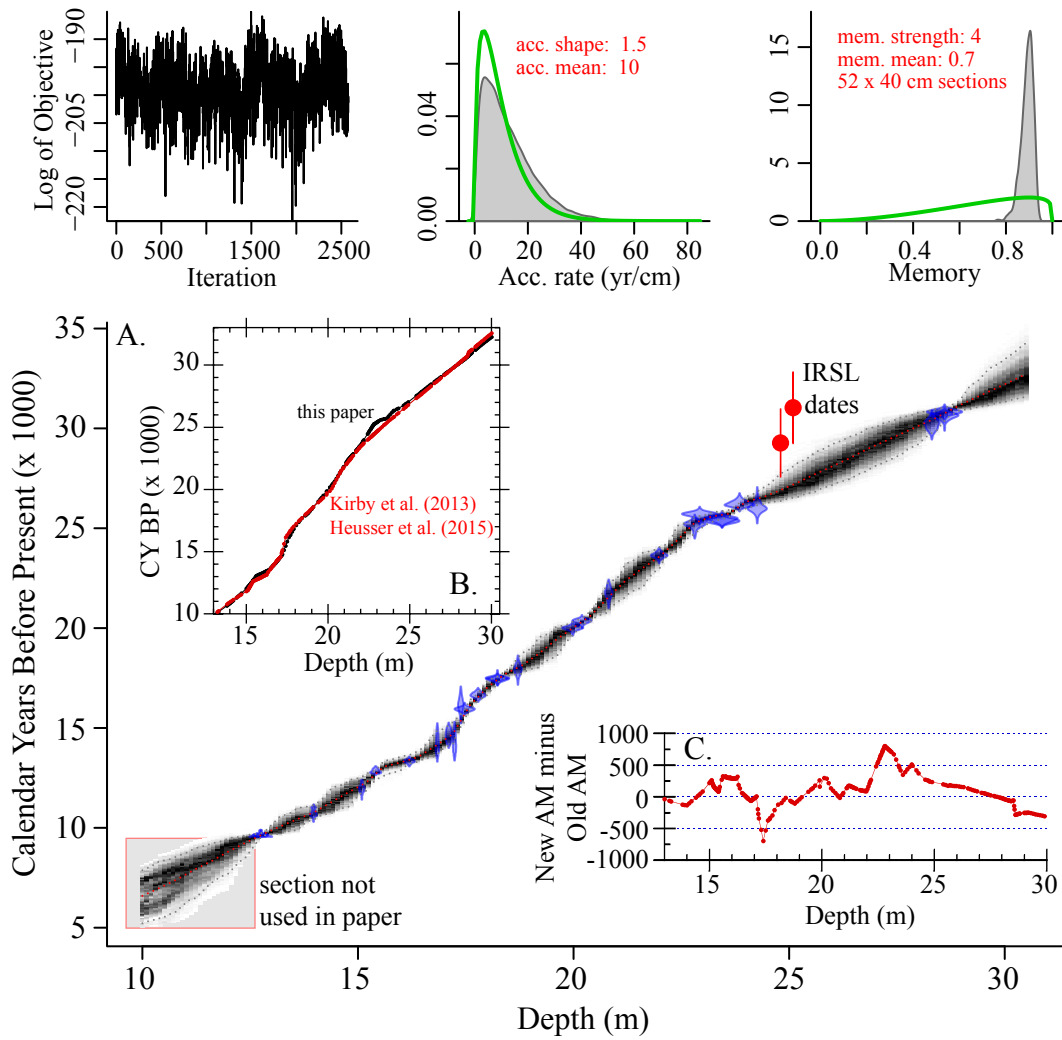


Figure 2

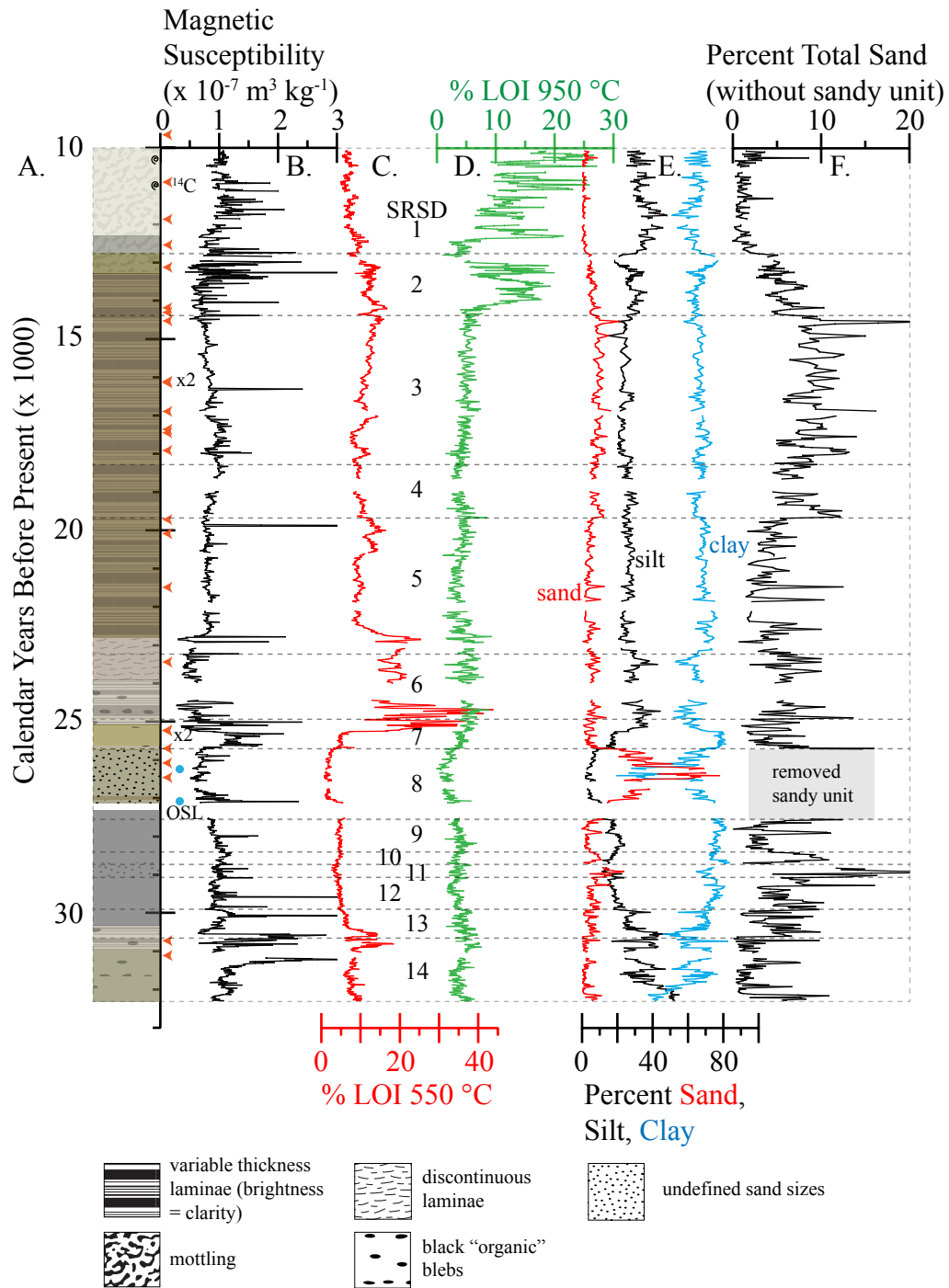


Figure 3

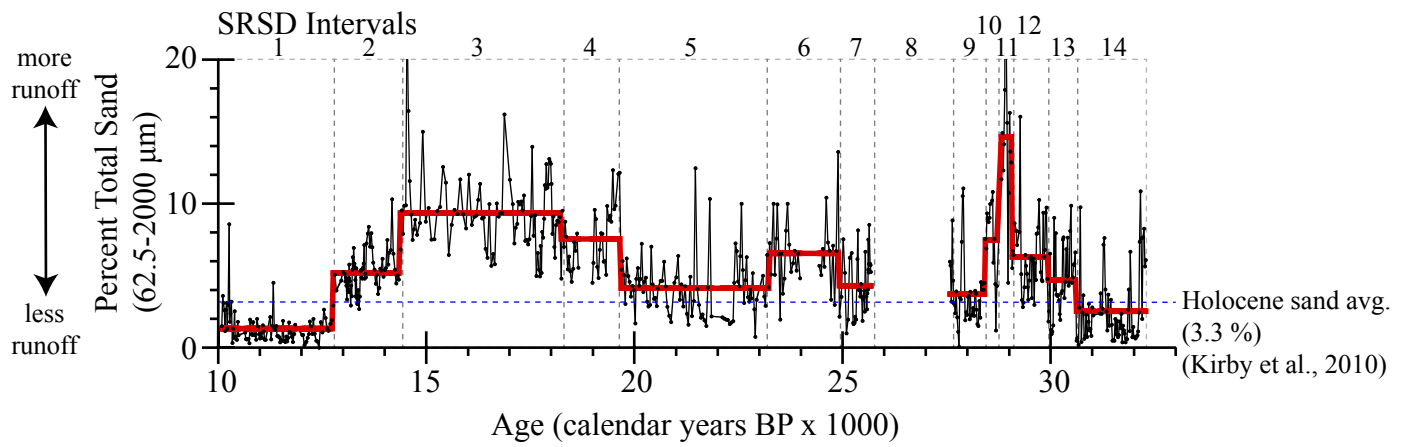


Figure 4

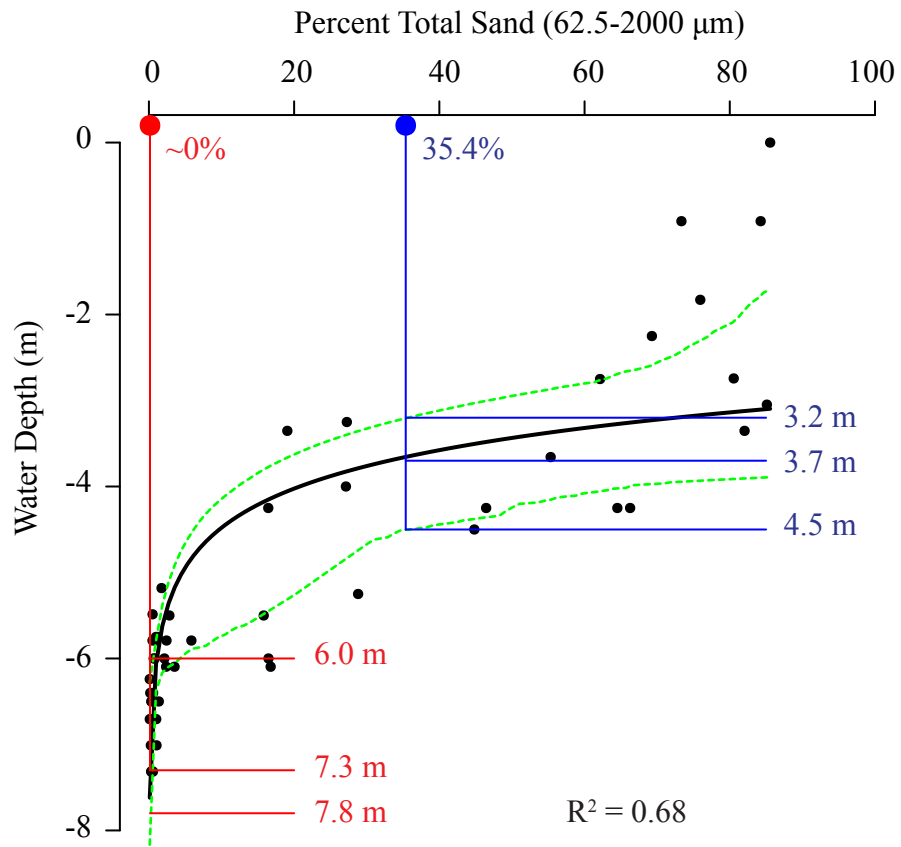


Figure 5

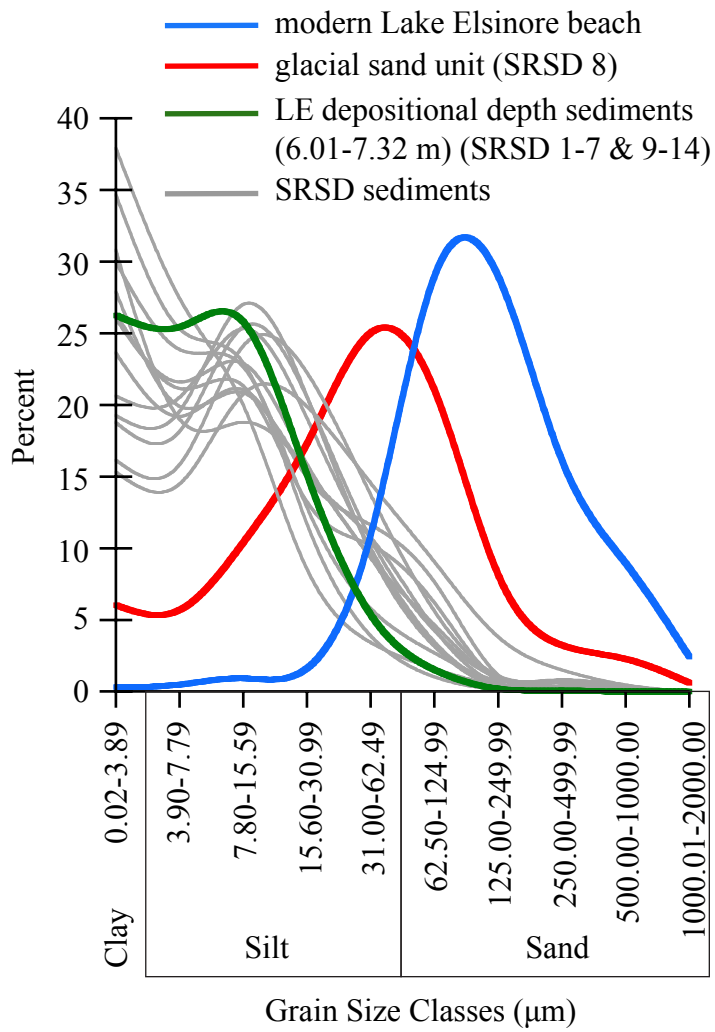


Figure 6

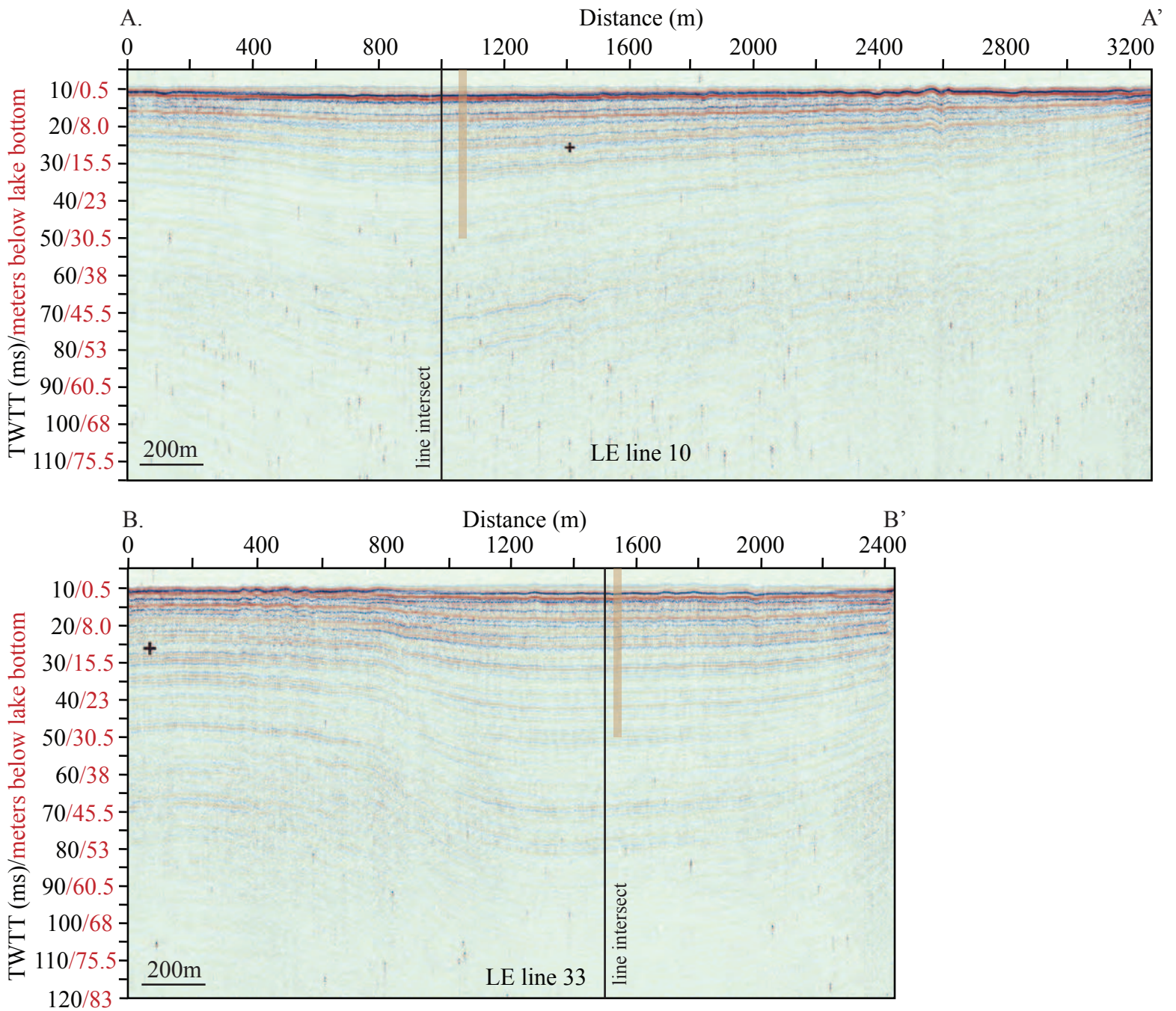
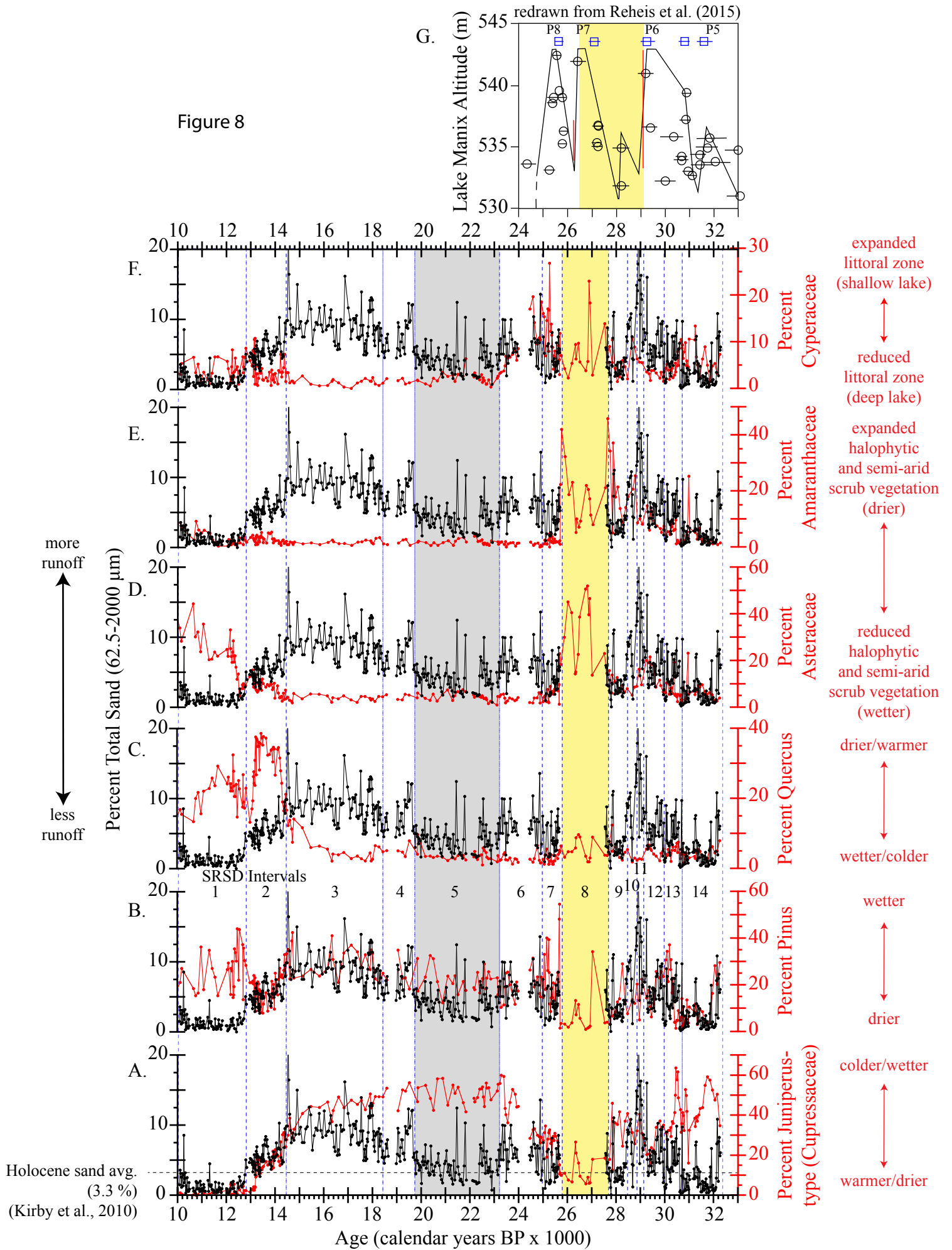


Figure 7

Figure 8



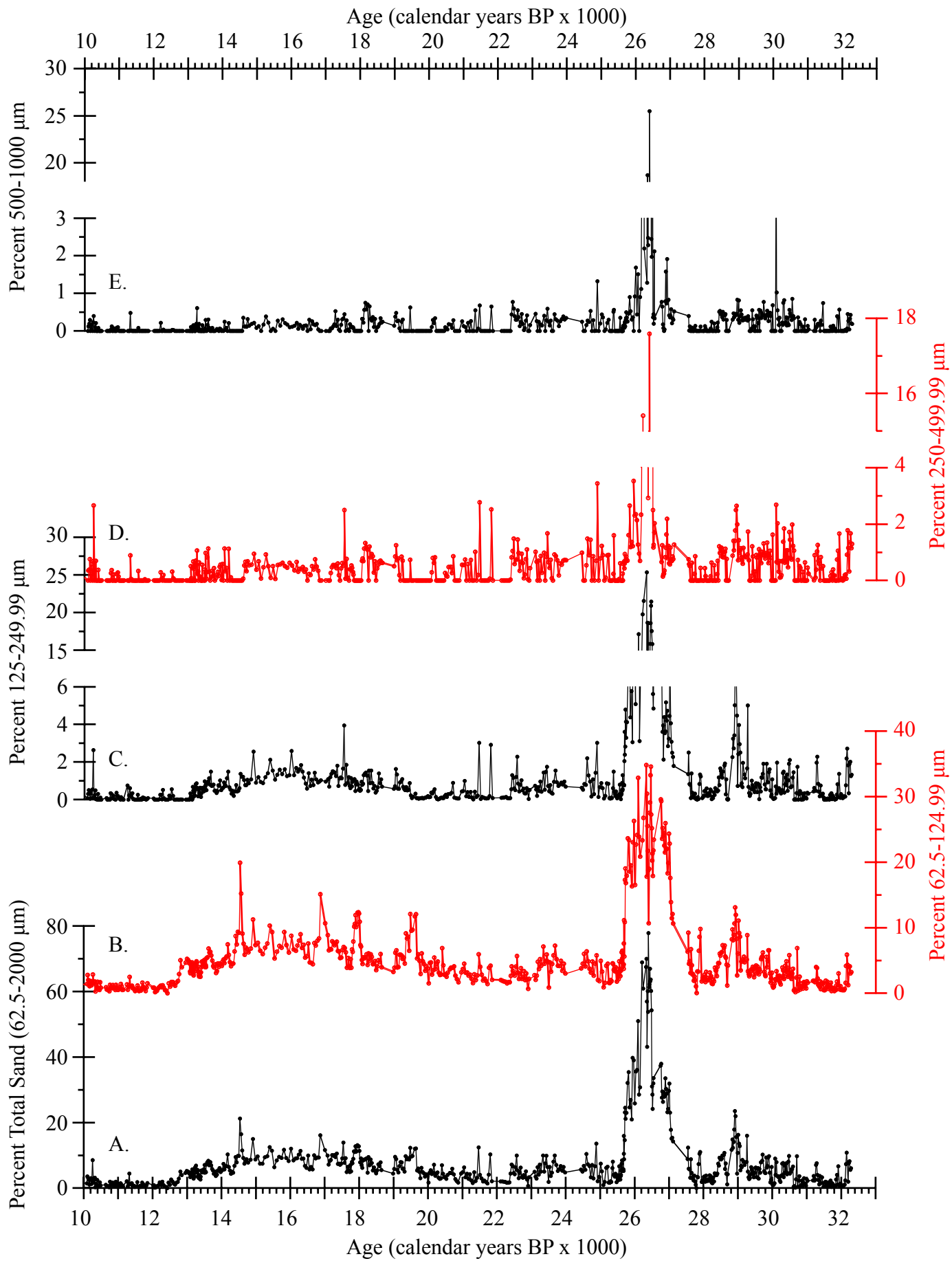


Figure S1

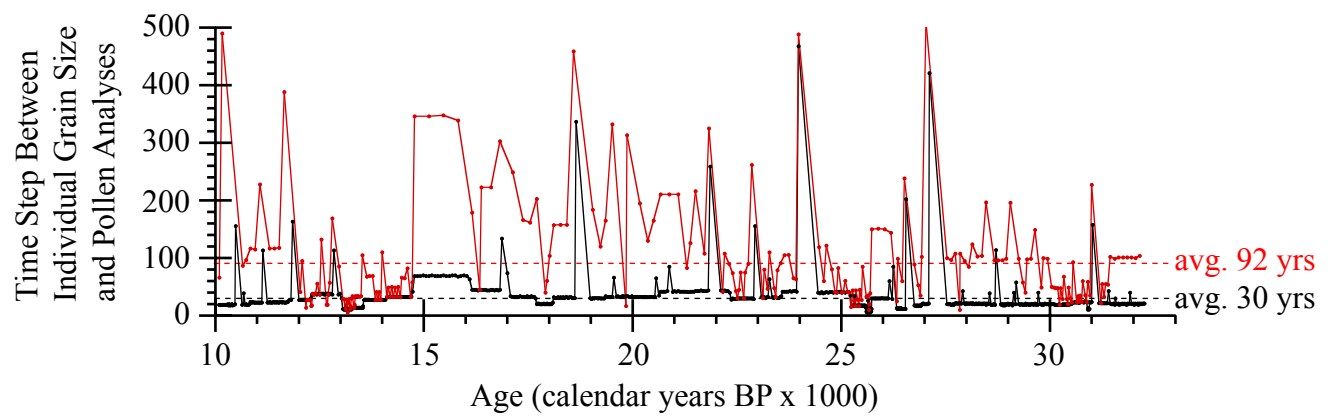


Figure S2